

Efficient Temporal Pattern Mining in Big Time Series Using Mutual Information

Van Long Ho, Nguyen Ho, Torben Bach Pedersen
Aalborg University, Denmark
{vlh,ntth,tbp}@cs.aau.dk

ABSTRACT

Very large time series are increasingly available from an ever wider range of IoT-enabled sensors deployed in different environments. Significant insights can be obtained through mining temporal patterns from these time series. Unlike traditional pattern mining, temporal pattern mining (TPM) adds additional temporal aspect, e.g., the time intervals of the events, into extracted patterns, making them more expressive. However, adding this extra temporal information to the patterns also adds an additional exponential factor to the exponential growth of the search space, increases significantly the mining complexity. This raises an imperative need to have a more efficient and scalable method for temporal pattern mining. Existing TPM methods either cannot scale to large datasets, or work only on pre-processed temporal events rather than on time series. This paper presents our comprehensive Frequent Temporal Pattern Mining from Time Series (FTPMfTS) with the following contributions: (1) The end-to-end FTPMfTS process that directly takes time series as input and produces frequent temporal patterns as output. (2) The efficient Hierarchical Temporal Pattern Graph Mining (HTPGM) algorithm that uses efficient data structures to enable fast computations of support and confidence, and employs effective pruning techniques to achieve significantly faster mining. (3) An approximate version of HTPGM which relies on mutual information to prune unpromising time series, and thus significantly reduce the search space. (4) An extensive experimental evaluation on synthetic and real-world datasets shows that HTPGM outperforms the baselines in runtime and memory consumption, and can scale to big datasets. The approximate HTPGM achieves up to 2 orders of magnitude speedup compared to the baselines while having high accuracy compared to the exact HTPGM.

1 INTRODUCTION

Rapid advancements in IoT technology have enabled the collection of enormous amounts of time series at unprecedented scale and speed. For example, modern residential households are now equipped with smart meters and smart plugs to enable fine-grained monitoring on the energy usage of the electrical appliances, weather stations have thousands of sensors to monitor hundreds of different weather-related variables, and mobile devices carry various sensors to track user behaviors and locations. These IoT-based systems are generating terabytes of data daily that contain rich information and once unlocked, can offer new insights into the application domains to support evidence-based decision making and optimization.

One of the first steps to uncover hidden patterns and extract new insights from time series data is to analyze patterns from them. Consider for example the time series in Fig. 1 that shows the energy usage of electrical appliances in a residential household. From Fig. 1, a pattern of activations between Clothes Washer, Dryer and Iron

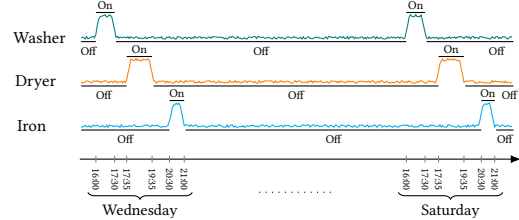


Figure 1: Energy usage time series of electrical devices

can be identified, showing that these appliances are often used together, usually on Wednesday and Saturday evening. Extracting such patterns is the task of pattern mining. However, traditional pattern mining methods do not fully capture the temporal dimension of the data. For example, sequential pattern would express the relation between appliances in Fig. 1 as $\{Washer\ On\} \Rightarrow \{Dryer\ On,\ Iron\ On\}$, indicating only the sequential occurrences of the events. Such patterns omit the pattern *occurrence times* which contain important information. To overcome this limitation, *temporal pattern mining* (TPM) adds the temporal information into the patterns, and thus, provides further details on when the relations between events happen, and for how long. For example, TPM can express the previous pattern more informatively as: $[16:00, 17:30] Washer\ On \Rightarrow [17:35, 19:35] Dryer\ On \Rightarrow [20:30, 21:00] Iron\ On$.

Temporal patterns can be found in most time series data from single or cross-domains. We demonstrate their usefulness below.

Example 1. In the energy domain, analyzing temporal patterns from residential energy usage time series can reveal how residents interact with electrical devices, and from that, understand their living habits. This allows to optimize the energy consumption. For example, knowing that the group of appliances $\{Clothes\ Washer,\ Dryer,\ Iron\}$ are often used together at $[16:00-21:00]$ every Wed and Sat would allow to automatically shift the operations of the Clothes Washer and Dryer to a time when the CO2 intensity of the electricity is low, e.g., due to large available amounts of solar or wind power, and do the ironing afterwards. This will (typically) reduce both electrical cost and CO2 emissions.

Example 2. In the smart city domain, temporal patterns extracted from joined weather and traffic time series can reveal the connection between weather conditions and collision severities. For instance, if a pattern: $[15:00, 17:00] Heavy\ Rain \Rightarrow [16:30, 19:00] High\ Motorist\ Injury$ is found with high confidence, then there is an increased risk of accidents after a heavy rain. Such patterns can assist to warn the drivers and thus reduce accidents.

Although temporal patterns are useful, mining them is much more expensive than sequential patterns. Not only does the temporal information adds extra computation to the mining process, the complex relations between events also add an additional exponential factor $O(3^{h^2})$ to the complexity $O(m^h)$ of the search space (m is the number of events and h is the length of temporal patterns),

yielding an overall complexity of $O(m^h 3^{h^2})$. Existing work such as [8, 24, 25], has tried to either use different representations to reduce the relation complexity, e.g., augmented representation, or propose different optimizations to improve TPM performance. However, these methods do not scale on big datasets, i.e., many attributes and many sequences, and/or do not work directly on time series but rather on pre-processed temporal events.

Contributions. In the present paper, we present our comprehensive Frequent Temporal Pattern Mining from Time Series (FTPMfTS) approach which overcomes the above limitations. Our key contributions are: (1) We present the first end-to-end FTPMfTS process that receives a set of time series as input, and produces frequent temporal patterns as output. Within this process, a splitting strategy is proposed to convert time series into event sequences while ensuring the preservation of temporal patterns. (2) We propose an efficient Hierarchical Temporal Pattern Graph Mining (HTPGM) algorithm to mine frequent temporal patterns which has several important novelties. First, HTPGM employs efficient data structures, Hierarchical Pattern Graph and *bitmap*, to enable fast computations of support and confidence. Second, two groups of pruning techniques based on the Apriori principle and the transitivity property of temporal relations are proposed to enable faster mining. (3) Based on mutual information, we propose a novel approximation version of HTPGM that prunes unpromising time series to significantly reduce the search space. The approximate HTPGM can scale on big datasets, i.e., many attributes and sequences. (4) We perform extensive experiments on synthetic and real-world datasets from various domains which show that HTPGM outperforms the baselines in both runtime and memory usage. The approximate HTPGM achieves up to 2 orders of magnitude speedup w.r.t. the baselines, while obtaining high accuracy compared to the exact HTPGM.

Paper outline. Section 2 covers related work. Section 3 defines the problem. Sections 4 and 5 present the exact and the approximate HTPGM. Section 6 shows the experimental evaluation and Section 7 concludes the paper and points to future work.

2 RELATED WORK

Temporal pattern mining: Compared to sequential pattern mining, TPM is rather a new research area. One of the first papers in this area is Kam et al. [15] that uses a hierarchical representation to manage temporal relations, and based on that mines temporal patterns. However, the approach in [15] suffers from ambiguity when presenting temporal relations. To overcome this, Wu et al. [26] define new non-ambiguous temporal relations, and develop TPrefix to mine temporal patterns. However, TPrefix has several inherent limitations: it scans the database repeatedly, and the algorithm does not employ any pruning strategies to reduce the search space. In [21], Moskovitch et al. design a TPM algorithm using the transitivity property of temporal relations. They use this property to generate candidates by inferring new relations between events. In comparison, our HTPGM uses the transitivity property for effective pruning. In [3], Iyad et al. propose a TPM framework to detect events in time series. However, their focus is to find irregularities in the data. Other work such as [4] proposes a TPM algorithm to classify health record data, while [7] introduces a condition TPM method to characterize pediatric asthma. However, these approaches are very domain-specific, and thus cannot generalize to other domains.

The state-of-the-art methods that currently achieve the best performance in TPM are H-DFS [24], TPMiner [8], and IEMiner [25]. H-DFS, proposed by Papapetrou et al., is a hybrid algorithm that uses bread-first and depth-first search strategies to mine frequent arrangements of temporal intervals. H-DFS uses a data structure called ID-List to transform event sequences into vertical representations, and temporal patterns are generated by merging the ID-Lists of different events. This means that H-DFS does not scale well when the number of data attributes increases. In [25], Patel et al. design a hierarchical lossless representation to model event relations, and propose IEMiner that uses Apriori-based optimizations to efficiently mine patterns from this new representation. In [8], Chen et al. propose TPMiner that uses endpoint and endtime representations to simplify the complex relations among events. Similar to [24], IEMiner and TPMiner do not scale to many data attributes. Our HTPGM algorithm improves on these methods by: (1) using efficient data structures and applying pruning techniques based on the Apriori principle and the transitivity property of temporal relations to enable fast mining, (2) the approximate HTPGM can handle datasets with many attributes and sequences, and (3), providing an end-to-end FTPMfTS process to mine temporal patterns directly from time series, a feature that is not supported by the baselines.

Using correlations in TPM: There have been attempts of applying different correlation measures such as expected support [1], all-confidence [18], and mutual information (MI) [6, 11, 16, 27] to optimize the pattern mining process. However, these only support sequential patterns. To the best of our knowledge, our proposed approximate HTPGM is the first that uses MI to optimize TPM.

3 PRELIMINARIES

3.1 Temporal Event of Time Series

Definition 3.1 (Time series) A *time series* $X = x_1, x_2, \dots, x_n$ is a sequence of data values that measure the same phenomenon during an observation time period, and are chronologically ordered.

Definition 3.2 (Symbolic time series) A *symbolic time series* X_S of a time series X encodes the raw values of X into a sequence of symbols. The finite set of permitted symbols used to encode X is called the *symbol alphabet* of X , denoted as Σ_X .

The symbolic time series X_S is obtained using a mapping function $f: X \rightarrow \Sigma_X$ that maps each value $x_i \in X$ to a symbol $\omega \in \Sigma_X$. For example, let $X = 1.61, 1.21, 0.41, 0.0$ be a time series representing the energy usage of an electrical device. Using the symbol alphabet $\Sigma_X = \{\text{On}, \text{Off}\}$, where On represents that the device is on and operating (e.g., $x_i \geq 0.5$), and Off that the device is off ($x_i < 0.5$), the symbolic representation of X is: $X_S = \text{On}, \text{On}, \text{Off}, \text{Off}$. The mapping function f can be defined using existing time series representation techniques such as SAX [19] or MVQ [20].

Definition 3.3 (Symbolic database) Given a set of time series $\mathcal{X} = \{X_1, \dots, X_n\}$, the set of symbolic representations of the time series in \mathcal{X} forms a *symbolic database* \mathcal{D}_{SYB} .

An example of the symbolic database \mathcal{D}_{SYB} is shown in Table 1. There are 6 time series representing the energy usage of 6 electrical appliances: {Stove, Toaster, Microwave, Clothes Washer, Dryer, Iron}. For brevity, we name the appliances respectively as {S, T, M, W, D, I}. All appliances have the same alphabet $\Sigma = \{\text{On}, \text{Off}\}$.

Definition 3.4 (Temporal event in a symbolic time series) A *temporal event* E in a symbolic time series X_S is a tuple $E = (\omega, T)$ where

Table 1: A Symbolic Database \mathcal{D}_{SYB}

Time	10:00	10:05	10:10	10:15	10:20	10:25	10:30	10:35	10:40	10:45	10:50	10:55	11:00	11:05	11:10	11:15	11:20	11:25	11:30	11:35	11:40	11:45	11:50	11:55	12:00	12:05	12:10	12:15	12:20	12:25	12:30	12:35	12:40	12:45	12:50	12:55	
S	On	On	On	On	Off	Off	Off	On	On	Off	Off	Off	Off	Off	On	On	On	On	Off	Off	Off	Off	On	On	On	Off	Off	On	On	Off	Off	On	On	On	Off	Off	
T	Off	On	On	On	Off	Off	Off	On	On	Off	Off	On	On	Off	Off	On	On	On	Off	Off	Off	Off	On	On	On	Off	Off	On	On	Off	Off	Off	On	On	On	Off	
M	Off	Off	Off	Off	On	On	On	Off	Off	On	On	On	Off	On	On	Off	Off	Off	On	On	Off	On	On	Off	Off	On	On	Off	Off	On	On	On	Off	Off	Off	On	On
W	Off	Off	Off	Off	On	On	On	Off	Off	On	On	Off	On	On	On	Off	Off	Off	On	On	Off	On	On	Off	Off	On	On	Off	Off	On	On	On	Off	Off	Off	On	On
D	Off	On	On	Off	Off	Off	Off	Off	On	On	Off	On	On	Off	Off	Off	Off	On	On	Off	Off																
I	Off	On	On	Off	On	On	Off	On	On	Off	Off	Off	Off	Off	Off	On	On																				

Table 2: Temporal Relations between Events

Follows: $E_{i \triangleright e_i} \rightarrow E_{j \triangleright e_j}$	
Contains: $E_{i \triangleright e_i} \triangleright E_{j \triangleright e_j}$	
Overlaps: $E_{i \triangleright e_i} \not\triangleright E_{j \triangleright e_j}$	

Table 3: A Temporal Sequence Database \mathcal{D}_{SEQ}

ID	Temporal sequences
1	(SON,[10:00,10:15]), (TOFF,[10:00,10:05]), (MOFF,[10:00,10:20]), (WOFF,[10:00,10:20]), (DOFF,[10:00,10:40]), (IOFF,[10:00,10:35]), (TON,[10:05,10:15]), (SOFF,[10:15,10:35]), (TOFF,[10:15,10:35]), (MON,[10:20,10:30]), (WON,[10:20,10:30]), (WOFF,[10:30,10:40]), (MOFF,[10:30,10:40]), (SON,[10:35,10:40]), (TON,[10:35,10:40]), (ION,[10:35,10:40])
2	(SOFF,[10:45,11:15]), (TOFF,[10:45,10:55]), (MON,[10:45,10:55]), (WON,[10:45,10:50]), (DON,[10:45,10:50]), (IOFF,[10:45,11:25]), (WOFF,[10:50,11:00]), (DOFF,[10:50,11:20]), (MOFF,[10:55,11:05]), (TON,[10:55,11:00]), (TOFF,[11:00,11:15]), (WON,[11:00,11:10]), (MON,[11:05,11:10]), (WOFF,[11:10,11:25]), (MOFF,[11:10,11:25]), (SON,[11:15,11:25]), (TON,[11:15,11:25]), (DON,[11:20,11:25])
3	(SOFF,[11:30,11:50]), (TOFF,[11:30,11:50]), (MON,[11:30,11:35]), (WON,[11:30,11:35]), (DOFF,[11:30,12:10]), (ION,[11:30,11:35]), (IOFF,[11:35,12:10]), (MOFF,[11:35,11:45]), (WOFF,[11:35,11:45]), (WON,[11:45,11:50]), (MON,[11:45,11:50]), (SON,[11:50,12:00]), (MOFF,[11:50,12:05]), (TON,[11:50,12:00]), (WOFF,[11:50,12:05]), (SOFF,[12:00,12:10]), (TOFF,[12:00,12:10]), (MON,[12:05,12:10]), (WON,[12:05,12:10])
4	(SON,[12:15,12:20]), (TON,[12:15,12:20]), (MOFF,[12:15,12:25]), (WOFF,[12:15,12:25]), (DON,[12:15,12:20]), (ION,[12:15,12:20]), (IOFF,[12:20,12:50]), (DOFF,[12:20,12:40]), (TOFF,[12:20,12:40]), (SOFF,[12:20,12:35]), (WON,[12:25,12:35]), (MON,[12:25,12:35]), (MOFF,[12:35,12:50]), (SON,[12:35,12:45]), (WOFF,[12:35,12:50]), (TON,[12:40,12:50]), (DON,[12:40,12:45]), (DOFF,[12:45,12:55]), (SOFF,[12:45,12:55]), (TOFF,[12:50,12:55]), (MON,[12:50,12:55]), (WON,[12:50,12:55]), (ION,[12:50,12:55])

$\omega \in \Sigma_X$ is a symbol, and $T = \{[t_{s_i}, t_{e_i}]\}$ is the set of time intervals during which X_S is associated with the symbol ω .

Given a time series X , a temporal event is created by first converting X into symbolic time series X_S , and then combining identical consecutive symbols in X_S into one single time interval. For example, consider the symbolic representation of S in Table 1. By combining its consecutive On symbols, we form the temporal event “Stove is On” as: (SON, $\{[10:00, 10:15], [10:35, 10:40], [11:15, 11:25], [11:50, 12:00], [12:15, 12:20], [12:35, 12:45]\}$).

Definition 3.5 (Instance of a temporal event) Let $E = (\omega, T)$ be a temporal event, and $[t_{s_i}, t_{e_i}] \in T$ be a time interval. The tuple $e = (\omega, [t_{s_i}, t_{e_i}])$ is called an *instance* of the event E , representing a single occurrence of E during $[t_{s_i}, t_{e_i}]$. We use the notation $E_{\triangleright e}$ to denote that event E has an instance e .

3.2 Relations between Temporal Events

We adopt the popular Allen’s relations model [2] and define three basic temporal relations between events. Furthermore, to avoid the exact time mapping problem in Allen’s relations, we adopt the *buffer* idea from [24], adding a tolerance *buffer* ϵ to the relation’s endpoints. However, we change the way ϵ is used in [24] to ensure the relations are *mutually exclusive* (proof is in the full paper [14]).

Consider two temporal events E_i and E_j , and their corresponding instances, $e_i = (\omega_i, [t_{s_i}, t_{e_i}])$ and $e_j = (\omega_j, [t_{s_j}, t_{e_j}])$. Let ϵ be a non-negative number ($\epsilon \geq 0$) representing the buffer size. The following relations can be defined between E_i and E_j through e_i and e_j .

Definition 3.6 (Follows) E_i and E_j form a *Follows* relation through e_i and e_j , denoted as Follows($E_{i \triangleright e_i}, E_{j \triangleright e_j}$) or $E_{i \triangleright e_i} \rightarrow E_{j \triangleright e_j}$, iff $t_{e_i} \pm \epsilon \leq t_{s_j}$.

Definition 3.7 (Contains) E_i and E_j form a *Contains* relation through e_i and e_j , denoted as Contains($E_{i \triangleright e_i}, E_{j \triangleright e_j}$) or $E_{i \triangleright e_i} \triangleright E_{j \triangleright e_j}$, iff $(t_{s_i} \leq t_{s_j}) \wedge (t_{e_i} \pm \epsilon \geq t_{e_j})$.

Definition 3.8 (Overlaps) E_i and E_j form an *Overlaps* relation through e_i and e_j , denoted as Overlaps($E_{i \triangleright e_i}, E_{j \triangleright e_j}$) or $E_{i \triangleright e_i} \not\triangleright E_{j \triangleright e_j}$, iff $(t_{s_i} < t_{s_j}) \wedge (t_{e_i} \pm \epsilon < t_{e_j}) \wedge (t_{e_i} - t_{s_j} \geq d_0 \pm \epsilon)$, where d_0 is the minimal overlapping duration between two event instances, and $0 \leq \epsilon \ll d_0$.

The *Follows* relation represents sequential occurrences of one event after another. For example, $E_{i \triangleright e_i}$ is followed by $E_{j \triangleright e_j}$ if the end time t_{e_i} of e_i occurs before the start time t_{s_j} of e_j . Here, the buffer ϵ is used as a tolerance, i.e., the *Follows* relation between $E_{i \triangleright e_i}$ and $E_{j \triangleright e_j}$ holds if $(t_{e_i} + \epsilon)$ or $(t_{e_i} - \epsilon)$ occurs before t_{s_j} . On the other hand, in a *Contains* relation, one event occurs entirely within the timespan of another event. Finally, in an *Overlaps* relation, the timespans of the two occurrences overlap each other.

Since the relations between events are formed through their instances, it is possible that the same event pair forms different relations through different instances. Moreover, an event can form a relation with itself. In this case, we call it a *self-relation*. Table 2 illustrates the three temporal relations and their conditions.

3.3 Temporal Pattern

Definition 3.9 (Temporal sequence) A list of n event instances $S = \langle e_1, \dots, e_i, \dots, e_n \rangle$ forms a *temporal sequence* if the instances are chronologically ordered by their start times. Moreover, S has size n , denoted as $|S| = n$.

Definition 3.10 (Temporal sequence database) A set of temporal sequences forms a *temporal sequence database* \mathcal{D}_{SEQ} where each row i contains a temporal sequence S_i .

Table 3 shows the temporal sequence database \mathcal{D}_{SEQ} , created from the symbolic database \mathcal{D}_{SYB} in Table 1.

Definition 3.11 (Temporal pattern) Let $\mathfrak{R} = \{\text{Follows, Contains, Overlaps}\}$ be the set of temporal relations. A *temporal pattern* $P = \langle (r_{12}, E_1,$

$(E_2), \dots, (r_{(n-1)(n)}, E_{n-1}, E_n)$ is a list of triples (r_{ij}, E_i, E_j) , each representing a relation $r_{ij} \in \mathfrak{R}$ between two events E_i and E_j .

Note that the relation r_{ij} in each triple is formed using the specific instances of E_i and E_j . A temporal pattern that has n events is called an n -event pattern. We use $E_i \in P$ to denote that the event E_i occurs in P , and $P_1 \subseteq P$ to say that a pattern P_1 is a sub-pattern of P .

Definition 3.12 (Temporal sequence supports a pattern) Let $S = \langle e_1, \dots, e_i, \dots, e_n \rangle$ be a temporal sequence. We say that S supports a temporal pattern P , denoted as $P \in S$, iff $|S| \geq 2 \wedge \forall (r_{ij}, E_i, E_j) \in P, \exists (e_l, e_m) \in S$ such that r_{ij} holds between $E_{i \rightarrow e_l}$ and $E_{j \rightarrow e_m}$.

If P is supported by S , P can be written as $P = \langle (r_{12}, E_{1 \rightarrow e_1}, E_{2 \rightarrow e_2}), \dots, (r_{(n-1)(n)}, E_{n-1 \rightarrow e_{n-1}}, E_{n \rightarrow e_n}) \rangle$, where the relation between two events in each triple is expressed using the event instances.

In Fig. 1, consider the temporal sequence $S = \langle e_1 = (\text{WOn}, [16:00, 17:30]), e_2 = (\text{DOn}, [17:35, 19:35]), e_3 = (\text{IOOn}, [20:30, 21:00]) \rangle$ representing the order of activations between Clothes Washer, Dryer, and Iron. Here, S supports a 3-event pattern $P = \langle (\text{Follows}, \text{WOn} \rightarrow e_1, \text{DOn} \rightarrow e_2), (\text{Follows}, \text{WOn} \rightarrow e_1, \text{IOOn} \rightarrow e_3), (\text{Follows}, \text{DOn} \rightarrow e_2, \text{IOOn} \rightarrow e_3) \rangle$.

Maximal duration constraint: Let $P \in S$ be a temporal pattern supported by the sequence S . The duration between the start time of the instance e_1 , and the end time of the instance e_n in S must not exceed the predefined maximal time duration t_{\max} : $t_{e_n} - t_{e_1} \leq t_{\max}$.

The maximal duration constraint guarantees that the relation between any two events is temporally valid. This enables the pruning of invalid patterns. For example, under this constraint, a *Follows* relation between a “Washer On” event and a “Dryer On” event happening one year apart should be considered invalid.

3.4 Frequent Temporal Pattern

Given a temporal sequence database \mathcal{D}_{SEQ} , we want to find patterns that occur frequently in \mathcal{D}_{SEQ} . We use *support* and *confidence* [23] to measure the frequency and the likelihood of a pattern. Note that unlike association rules, temporal patterns do not have antecedents and consequents. Instead, they represent pair-wise temporal relations between events based on their temporal occurrences.

Definition 3.13 (Support of a temporal event) The *support* of a temporal event E in \mathcal{D}_{SEQ} is the number of sequences $S \in \mathcal{D}_{\text{SEQ}}$ which contain at least one instance e of E .

$$\text{supp}(E) = |\{S \in \mathcal{D}_{\text{SEQ}} \text{ s.t. } \exists e \in S : E \rightarrow e\}| \quad (1)$$

The *relative support* of E is the fraction between $\text{supp}(E)$ and the size of \mathcal{D}_{SEQ} :

$$\text{rel-supp}(E) = \text{supp}(E) / |\mathcal{D}_{\text{SEQ}}| \quad (2)$$

Similarly, the support of a group of events (E_1, \dots, E_n) , denoted as $\text{supp}(E_1, \dots, E_n)$, is the number of sequences $S \in \mathcal{D}_{\text{SEQ}}$ which contain at least one instance (e_1, \dots, e_n) of the event group.

Definition 3.14 (Support of a temporal pattern) The *support* of a pattern P is the number of sequences $S \in \mathcal{D}_{\text{SEQ}}$ that support P .

$$\text{supp}(P) = |\{S \in \mathcal{D}_{\text{SEQ}} \text{ s.t. } P \in S\}| \quad (3)$$

The *relative support* of P in \mathcal{D}_{SEQ} is the fraction

$$\text{rel-supp}(P) = \text{supp}(P) / |\mathcal{D}_{\text{SEQ}}| \quad (4)$$

Definition 3.15 (Confidence of an event pair) The *confidence* of an event pair (E_i, E_j) in \mathcal{D}_{SEQ} is the fraction between $\text{supp}(E_i, E_j)$ and the support of its most frequent event:

$$\text{conf}(E_i, E_j) = \frac{\text{supp}(E_i, E_j)}{\max\{\text{supp}(E_i), \text{supp}(E_j)\}} \quad (5)$$

Definition 3.16 (Confidence of a temporal pattern) The *confidence* of a temporal pattern P in \mathcal{D}_{SEQ} is the fraction between $\text{supp}(P)$ and the support of its most frequent event:

$$\text{conf}(P) = \frac{\text{supp}(P)}{\max_{1 \leq k \leq |P|} \{\text{supp}(E_k)\}} \quad (6)$$

where $E_k \in P$ is a temporal event. Since the denominator in Eq. (6) is the maximum support of the events in P , the confidence computed in Eq. (6) is the *minimum confidence* of a pattern P in \mathcal{D}_{SEQ} , representing how likely the pattern P (at least) is, given the occurrence of its most frequent event. The confidence in Eq. (6) is also called the *all-confidence* as in [23]. We are now ready to define the problem of mining frequent temporal patterns from time series.

Frequent Temporal Pattern Mining from Time Series (FTPMfTS). Given a set of time series $\mathcal{X} = \{X_1, \dots, X_n\}$, let \mathcal{D}_{SEQ} be the temporal sequence database obtained from \mathcal{X} , and σ and δ be the support and confidence thresholds, respectively. The FTPMfTS problem aims to find all temporal patterns P that have high enough support and confidence in \mathcal{D}_{SEQ} : $\text{supp}(P) \geq \sigma \wedge \text{conf}(P) \geq \delta$.

4 FREQUENT TEMPORAL PATTERN MINING

4.1 Overview of the FTPMfTS Process

Fig. 2 gives an overview of the FTPMfTS process which consists of 2 phases. The first phase, *Data Transformation*, converts a set of time series \mathcal{X} into a symbolic database \mathcal{D}_{SYB} , and then converts \mathcal{D}_{SYB} into a temporal sequence database \mathcal{D}_{SEQ} . The second phase, *Frequent Temporal Pattern Mining*, mines frequent patterns which includes 3 steps: (1) *Frequent Single Event Mining*, (2) *Frequent 2-Event Pattern Mining*, and (3) *Frequent k-Event Pattern Mining* ($k > 2$). The final output is a set of all frequent patterns in \mathcal{D}_{SEQ} .

4.2 Data Transformation

4.2.1 Symbolic Time Series Representation. Given a set of time series \mathcal{X} , the symbolic representation of each time series $X \in \mathcal{X}$ is obtained by using a mapping function as in Def. 3.2.

4.2.2 Temporal Sequence Database Conversion. To convert \mathcal{D}_{SYB} to \mathcal{D}_{SEQ} , a straightforward approach is to split the symbolic series in \mathcal{D}_{SYB} into equal-length sequences, each belongs to a row in \mathcal{D}_{SEQ} . For example, if each symbolic series in Table 1 is split into 4 sequences, then each sequence will last for 40 minutes. The first sequence S_1 of \mathcal{D}_{SEQ} therefore contains temporal events of S, T, M, W, D, and I from 10:00 to 10:40. The second sequence S_2 contains events from 10:45 to 11:25, and similarly for S_3 and S_4 .

However, the splitting can lead to a potential loss of temporal patterns. The loss happens when a *splitting point* accidentally divides a temporal pattern into different sub-patterns, and places these into separate sequences. We explain this situation in Fig. 3a. Consider 2 sequences S_1 and S_2 , each of length t . Here, the splitting point divides a pattern of 4 events, {SOn, TOn, MOn, WOn}, into two sub-patterns, in which SOn and TOn are placed in S_1 , and MOn and WOn in S_2 . This results in the loss of this 4-event pattern which can be identified only when all 4 events are in the same sequence.

To prevent such a loss, we propose a *splitting strategy* using overlapping sequences. Specifically, two consecutive sequences are overlapped by a duration t_{ov} : $0 \leq t_{\text{ov}} \leq t_{\max}$, where t_{\max} is the *maximal duration* of a temporal pattern. The value of t_{ov} decides how large the overlap between S_i and S_{i+1} is: $t_{\text{ov}} = 0$ results in no overlap, i.e., no redundancy, but with a potential loss of patterns, while $t_{\text{ov}} = t_{\max}$ creates large overlaps between sequences, i.e., high redundancy, but all patterns are preserved. As illustrated in Fig. 3b, the overlapping between S_1 and S_2 keeps the 4 events together in the same sequence S_2 , and thus helps preserve the pattern.

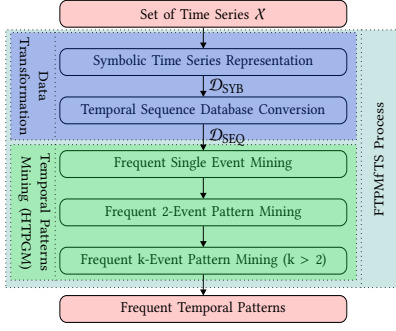


Figure 2: The FTPMfTS process

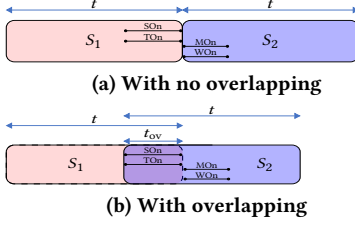


Figure 3: Splitting strategy

4.3 Frequent Temporal Patterns Mining

We now present our method, called Hierarchical Temporal Pattern Graph Mining (HTPGM), to mine frequent temporal patterns from \mathcal{D}_{SEQ} . The main novelties of HTPGM are: a) the use of efficient data structures, i.e., the proposed Hierarchical Pattern Graph and *bitmap indexing*, to enable fast computations of support and confidence, and b) the proposal of two groups of pruning techniques based on the Apriori principle and the temporal transitivity property of temporal events. In Section 5, we introduce an approximate version of HTPGM based on mutual information to further optimize the mining process. We first discuss the data structures used in HTPGM.

Hierarchical Pattern Graph (HPG): We use a hierarchical graph structure, called the *Hierarchical Pattern Graph*, to keep track of the frequent events and patterns found in each mining step. The HPG allows HTPGM to mine iteratively (e.g., 2-event patterns are mined based on frequent single events, 3-event patterns are mined based on 2-event patterns, and so on) and perform effective pruning. Fig. 4 shows the HPG built from \mathcal{D}_{SEQ} in Table 3: the root is the empty set \emptyset , and each level L_k maintains frequent k -event patterns. As HTPGM proceeds, HPG is constructed gradually. We explain this process for each mining step.

Efficient bitmap indexing: We use *bitmaps* to index the occurrences of events and patterns in \mathcal{D}_{SEQ} , enabling fast computations of support and confidence. Specifically, each event E or pattern P found in \mathcal{D}_{SEQ} is associated with a *bitmap* indicating where E or P occurs. Each *bitmap* b has length $|\mathcal{D}_{SEQ}|$ (i.e., the number of sequences), and has value $b[i] = 1$ if E or P is present in sequence i of \mathcal{D}_{SEQ} , or $b[i] = 0$ otherwise. An example *bitmap* can be seen at L_1 in Fig. 4. The event IO_{On} has the *bitmap* $b_{IO_{On}} = [1, 0, 1, 1]$, indicating that IO_{On} occurs in all but the second sequence of \mathcal{D}_{SEQ} .

Constructing the *bitmap* is also done step by step. For single events in \mathcal{D}_{SEQ} , *bitmaps* are built by scanning \mathcal{D}_{SEQ} only once. Algorithm 1 provides the pseudo-code of HTPGM. The details are explained in each mining step.

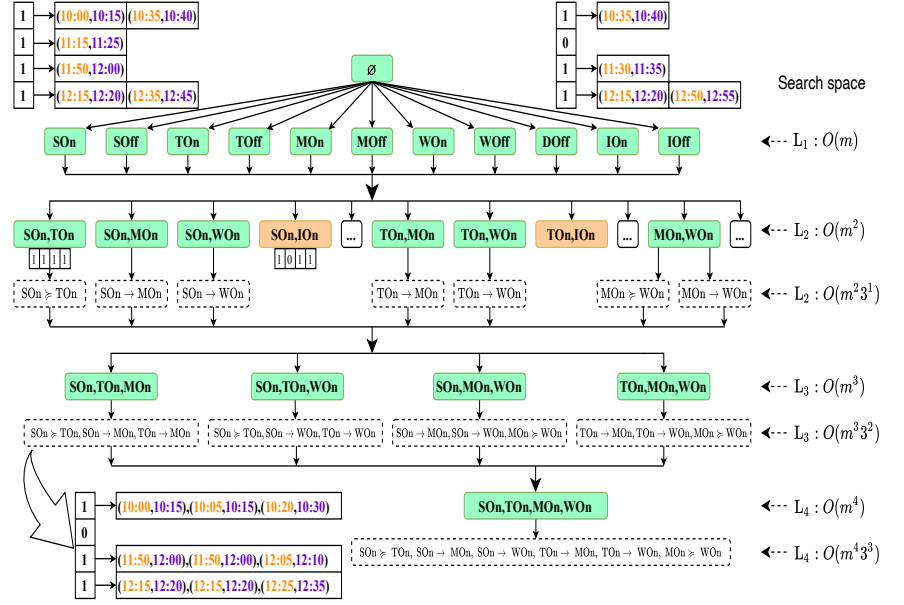


Figure 4: A Hierarchical Pattern Graph for Table 3

Algorithm 1: Hierarchical Temporal Pattern Graph Mining

Input: Temporal sequence database \mathcal{D}_{SEQ} , a support threshold σ , a confidence threshold δ

Output: The set of frequent temporal patterns P

// Mining frequent single events

- 1: **foreach** event $E_i \in \mathcal{D}_{SEQ}$ **do**
- 2: $supp(E_i) \leftarrow \text{countBitmap}(b_{E_i});$
- 3: **if** $supp(E_i) \geq \sigma$ **then**
- 4: Insert E_i to $1Freq$;

// Mining frequent 2-event patterns

- 5: EventPairs $\leftarrow \text{Cartesian}(1Freq, 1Freq)$;
- 6: FrequentPairs $\leftarrow \emptyset$;
- 7: **foreach** (E_i, E_j) in EventPairs **do**
- 8: $b_{ij} \leftarrow \text{AND}(b_{E_i}, b_{E_j});$
- 9: $supp(E_i, E_j) \leftarrow \text{countBitmap}(b_{ij});$
- 10: **if** $supp(E_i, E_j) \geq \sigma$ **then**
- 11: FrequentPairs $\leftarrow \text{Apply_Lemma3}(E_i, E_j)$;

foreach (E_i, E_j) in FrequentPairs **do**

- 12: Retrieve event instances;
- 13: Check frequent relations;

// Mining frequent k-event patterns

- 15: Filtered1Freq $\leftarrow \text{Transitivity_Filtering}(1Freq)$; //Lemmas 4, 5
- 16: kEventCombinations $\leftarrow \text{Cartesian}(\text{Filtered1Freq}, (k-1)Freq)$;
- 17: frequentkEvents $\leftarrow \text{Apriori_Filtering}(kEventCombinations)$;
- 18: **foreach** $kEvents$ in frequentkEvents **do**
- 19: Retrieve relations;
- 20: Iteratively check frequent relations; //Lemmas 4, 6, 7

4.4 Mining Frequent Single Events

The first step in HTPGM is to find frequent single events (Alg. 1, lines 1-4) which is easily done using the *bitmap*. For each event E_i in \mathcal{D}_{SEQ} , the support $supp(E_i)$ is computed by counting the number

of set bits in *bitmap* b_{E_i} , and comparing against σ . Note that for single events, *confidence* is not considered since it is always 1.

After this step, the set *IFreq* containing frequent single events is created to build L_1 of HPG. We illustrate this process using Table 3, with $\sigma = 0.7$ and $\delta = 0.7$. Here, *IFreq* contains 11 frequent events, each belongs to one node in L_1 . The event DOn is not frequent (only appears in sequences 2 and 4), and is thus omitted. Each L_1 node has a unique event name, a *bitmap*, and a list of instances corresponding to that event (see SOn at L_1).

Complexity: The complexity of finding frequent single events is $O(m \cdot |\mathcal{D}_{SEQ}|)$, where m is the number of distinct events.

Proof. Detailed proofs of all complexities, lemmas and theorems in this article can be found in the Appendix of the full paper [14].

4.5 Mining Frequent 2-event Patterns

4.5.1 Search space of HTPGM. The next step in HTPGM is to mine frequent 2-event patterns. A straightforward approach would be to enumerate all possible event pairs, and check whether each pair can form frequent patterns. However, this *naive* approach is very expensive. Not only does it need to repeatedly scan \mathcal{D}_{SEQ} to check each combination of events, the complex relations between events also add an extra exponential factor 3^{h^2} to the m^h number of possible candidates, creating a very large search space that makes the approach infeasible.

LEMMA 1. Let m be the number of distinct events in \mathcal{D}_{SEQ} , and h be the longest length of a temporal pattern. The total number of temporal patterns in HPG from L_1 to L_h is $O(m^h 3^{h^2})$.

As seen in Lemma 1, the HTPGM search space is driven by the number of the distinct events (m), the length of temporal patterns (h), and the number of temporal relations (3). A dataset of just a few hundred events can create a very large search space containing billions of candidate patterns. The optimizations and approximation proposed in the following sections help mitigate this problem.

4.5.2 Two-steps filtering approach. Given the huge set of pattern candidates, it is expensive to check their support and confidence. We propose a *filtering approach* to reduce the unnecessary candidate checking. Specifically, at any level l ($l \geq 2$) in HPG, the mining process is divided into two steps: (1) it first finds frequent nodes (i.e., remove infrequent combinations of events), (2) it then generates temporal patterns only from frequent nodes. The correctness of this filtering approach is based on the Apriori-inspired lemmas below.

LEMMA 2. Let P be a 2-event pattern formed by an event pair (E_i, E_j) . Then, $\text{supp}(P) \leq \text{supp}(E_i, E_j)$.

From Lemma 2, infrequent event pairs cannot form frequent patterns as the pattern support is at most the support of its events.

LEMMA 3. Let (E_i, E_j) be a pair of events occurring in a 2-event pattern P . Then $\text{conf}(P) \leq \text{conf}(E_i, E_j)$.

From Lemma 3, the confidence of a pattern P is always at most the confidence of its events. Thus, a low-confidence event pair cannot form any high-confidence patterns. We note that the Apriori principle has already been used in other work, e.g., [8, 24], for mining optimization. However, they only apply this principle to the support (Lemma 2), while we further extend it to the confidence (Lemma 3). Applying Lemmas 2 and 3 to the first filtering step will remove infrequent or low-confidence event pairs, reducing the candidate patterns of HTPGM. We detail this filtering below.

Step 2.1. Mining frequent event pairs: This step finds frequent event pairs in \mathcal{D}_{SEQ} , using the set *IFreq* found in L_1 of HPG (Alg. 1, lines 5-11). First, HTPGM generates all possible event pairs by calculating the Cartesian product $IFreq \times IFreq$. Next, for each pair (E_i, E_j) , the joint *bitmap* b_{ij} (representing the set of sequences where both events occur) is computed by *ANDing* the two individual bitmaps: $b_{ij} = \text{AND}(b_{E_i}, b_{E_j})$. Finally, HTPGM computes the support $\text{supp}(E_i, E_j)$ by counting the set bits in b_{ij} , and comparing against σ . If $\text{supp}(E_i, E_j) \geq \sigma$, (E_i, E_j) has high enough support. Next, (E_i, E_j) is further filtered using Lemma 3: (E_i, E_j) is selected only if its confidence is at least δ . After this step, only frequent and high-confidence event pairs remain and form the nodes in L_2 .

Step 2.2. Mining frequent 2-event patterns: This step finds frequent 2-event patterns from the nodes in L_2 (Alg. 1, lines 12-14). For each node $(E_i, E_j) \in L_2$, we use the *bitmap* b_{ij} to retrieve the set of sequences \mathcal{S} where both events are present. Next, for each sequence $S \in \mathcal{S}$, the pairs of event instances (e_i, e_j) are extracted, and the relations between them are verified. The support and confidence of each relation $r(E_{i \rightarrow e_i}, E_{j \rightarrow e_j})$ are computed and compared against the thresholds, after which only frequent relations are selected and stored in the corresponding node in L_2 . Examples of the relations in L_2 can be seen in Fig. 4, e.g., node (SOn, TOn).

Step 2.2 results in two different sets of nodes in L_2 . The first set contains nodes that have frequent events but do not have any frequent patterns. These nodes (colored in brown in Fig. 4) are removed from L_2 . The second set contains nodes that have both frequent events and frequent patterns (colored in green), which remain in L_2 and are used in the subsequent mining steps.

Complexity: Let m be the number of frequent single events in L_1 , and i be the average number of event instances of each frequent event. The complexity of frequent 2-event pattern mining is $O(m^2 i^2 |\mathcal{D}_{SEQ}|^2)$.

4.6 Mining Frequent k-event Patterns

Mining frequent k -event patterns ($k \geq 3$) follows a similar process as 2-event patterns, with additional prunings based on the transitivity property of temporal relations.

Step 3.1. Mining frequent k-event combinations: This step finds frequent k -event combinations in L_k (Alg. 1, lines 15-17).

Let $(k-1)Freq$ be the set of frequent $(k-1)$ -event combinations found in L_{k-1} , and *IFreq* be the set of frequent single events in L_1 . To generate all k -event combinations, the typical process is to compute the Cartesian product: $(k-1)Freq \times IFreq$. However, we observe that using *IFreq* to generate k -event combinations at L_k can create redundancy, since *IFreq* might contain events that when combined with nodes in L_{k-1} , result in combinations that clearly cannot form any frequent patterns. To illustrate this observation, consider node IOn at L_1 in Fig. 4. Here, IOn is a frequent event, and thus, can be combined with frequent nodes in L_2 such as (SOn, TOn) to create a 3-event combination (SOn, TOn, IOn). However, (SOn, TOn, IOn) cannot form any frequent 3-event patterns, since IOn is not present in any frequent 2-event patterns in L_2 . To reduce the redundancy, the combination (SOn, TOn, IOn) should not be created in the first place. We rely on the *transitivity property* of temporal relations to identify such event combinations.

LEMMA 4. Let $S = \langle e_1, \dots, e_{n-1} \rangle$ be a temporal sequence that supports an $(n-1)$ -event pattern $P = \langle (r_{12}, E_{1 \rightarrow e_1}, E_{2 \rightarrow e_2}), \dots, (r_{(n-2)(n-1)},$

$E_{n-2\epsilon_{n-2}}, E_{n-1\epsilon_{n-1}}) >$. Let e_n be a new event instance added to S to create the temporal sequence $S' = \langle e_1, \dots, e_n \rangle$.

The set of temporal relations \mathfrak{R} is transitive on S' : $\forall e_i \in S', i < n, \exists r \in \mathfrak{R}$ s.t. $r(E_{i\epsilon_{e_i}}, E_{n\epsilon_{e_n}})$ holds.

From Lemma 4, a new event instance always forms at least one temporal relation with existing instances of a sequence. Based on this transitivity property, we can prove the following lemma.

LEMMA 5. Let $N_{k-1} = (E_1, \dots, E_{k-1})$ be a frequent $(k-1)$ -event combination, and E_k be a frequent single event. The combination $N_k = N_{k-1} \cup E_k$ can form frequent k -event temporal patterns if $\forall E_i \in N_{k-1}, \exists r \in \mathfrak{R}$ s.t. $r(E_i, E_k)$ is a frequent temporal relation.

From Lemma 5, only single events in L_1 that form at least one frequent pattern in L_{k-1} should be used to create event combinations in L_k . Using this result, we perform an initial filtering on $1Freq$ ahead of the Cartesian product calculation. Specifically, from the nodes in L_{k-1} , we extract the distinct single events D_{k-1} , and intersect them with $1Freq$ to remove redundant single events: $Filtered1Freq = D_{k-1} \cap 1Freq$. Then, the Cartesian product $(k-1)Freq \times Filtered1Freq$ is calculated to generate all possible k -event combinations. Next, we apply Lemmas 2 and 3 to select only frequent and high-confidence k -event combinations $kFreq$ to form L_k .

Step 3.2 Mining frequent k -event patterns: This step finds frequent k -event patterns from the nodes in L_k (Alg. 1, lines 18-20). Unlike 2-event patterns, determining the relations in a k -event combination ($k \geq 3$) is much more expensive, as it requires to verify the frequency of $\frac{1}{2}k(k-1)$ triples. To reduce the cost of relation checking, we propose an iterative verification method that relies on the *transitivity property* and the *Apriori principle*.

LEMMA 6. Let P and P' be two temporal patterns. If $P' \subseteq P$, then $conf(P') \geq conf(P)$.

LEMMA 7. Let P and P' be two temporal patterns. If $P' \subseteq P$ and $\frac{supp(P')}{\max_{1 \leq k \leq |P|} \{supp(E_k)\}} \leq \delta$, then $conf(P) \leq \delta$.

From Lemmas 6 and 7, a temporal pattern P cannot be high-confidence if any of its sub-patterns are low-confidence.

Let $N_{k-1} = (E_1, \dots, E_{k-1})$ be a node in L_{k-1} , $N_1 = (E_k)$ be a node in L_1 , and $N_k = N_{k-1} \cup N_1 = (E_1, \dots, E_k)$ be a node in L_k . To find k -event patterns for N_k , we first retrieve the set P_{k-1} containing frequent $(k-1)$ -event patterns in node N_{k-1} . Each $p_{k-1} \in P_{k-1}$ is a list of $\frac{1}{2}(k-1)(k-2)$ triples: $\{(r_{12}, E_{1\epsilon_{e_1}}, E_{2\epsilon_{e_2}}), \dots, (r_{(k-2)(k-1)}, E_{k-2\epsilon_{e_{k-2}}}, E_{k-1\epsilon_{e_{k-1}}})\}$. We iteratively verify the possibility of p_{k-1} forming a frequent k -event pattern with E_k as follows.

We first check whether the triple $(r_{(k-1)k}, E_{k-1\epsilon_{e_{k-1}}}, E_{k\epsilon_{e_k}})$ is frequent and high-confidence by accessing the node (E_{k-1}, E_k) in L_2 . If the triple is not frequent (using Lemmas 4 and 5) or high-confidence (using Lemmas 4, 6, and 7), the verifying process stops immediately for p_{k-1} . Otherwise, it continues on the triple $(r_{(k-2)k}, E_{k-2\epsilon_{e_{k-2}}}, E_{k\epsilon_{e_k}})$, until it reaches $(r_{1k}, E_{1\epsilon_{e_1}}, E_{k\epsilon_{e_k}})$.

We note that the transitivity property of temporal relations has been exploited in [21] to generate new relations. Instead, we use this property to prune unpromising candidates (Lemmas 4, 5, 6, 7).

Complexity: Let r be the average number of frequent $(k-1)$ -event patterns in L_{k-1} . The complexity of frequent k -event pattern mining is $O(|1Freq| \cdot |L_{k-1}| \cdot r \cdot k^2 \cdot |\mathcal{D}_{SEQ}|)$.

HTPGM overall complexity: Throughout this section, we have seen that HTPGM complexity depends on the size of the search

space ($O(m^{h^3}3^{h^2})$) and the complexity of the mining process itself, i.e., $O(m \cdot |\mathcal{D}_{SEQ}|) + O(m^2 i^2 |\mathcal{D}_{SEQ}|^2) + O(|1Freq| \cdot |L_{k-1}| \cdot r \cdot k^2 \cdot |\mathcal{D}_{SEQ}|)$. While the parameters m, h, i, r and k depend on the number of attributes, others such as $|1Freq|, |L_{k-1}|$ and $|\mathcal{D}_{SEQ}|$ also depend on the number of temporal sequences. Thus, given a dataset, HTPGM complexity is driven by two main factors: the number of attributes and the number of temporal sequences. In Section 6, we vary these two factors to evaluate the scalability of our solutions.

5 APPROXIMATE HTPGM

In this section, we first use mutual information (MI) to define so-called *correlated* symbolic time series, and then use this concept to derive the confidence lower bound of an event pair. Based on the confidence lower bound, we propose an approximate version of HTPGM that mines frequent temporal patterns only from the *correlated* symbolic series, a subset of \mathcal{D}_{SYB} , which significantly reduces the search space. Our experiments in Section 6 show that the approximate HTPGM achieves high accuracy with much lower runtimes, since the *uncorrelated* symbolic series typically result in infrequent patterns with low confidence.

5.1 Correlated Symbolic Time Series

Let X_S and Y_S be the symbolic series representing the time series X and Y , respectively, and Σ_X, Σ_Y be their symbolic alphabets.

Definition 5.1 (Entropy) The *entropy* of X_S , denoted as $H(X_S)$, is defined as

$$H(X_S) = - \sum_{x \in \Sigma_X} p(x) \cdot \log p(x) \quad (7)$$

Intuitively, the entropy measures the amount of information or the inherent uncertainty in the possible outcomes of a random variable. The higher the $H(X_S)$, the more uncertain the outcome of X_S .

The conditional entropy $H(X_S|Y_S)$ quantifies the amount of information needed to describe the outcome of X_S , given the value of Y_S , and is defined as

$$H(X_S|Y_S) = - \sum_{x \in \Sigma_X} \sum_{y \in \Sigma_Y} p(x, y) \cdot \log \frac{p(x, y)}{p(y)} \quad (8)$$

Definition 5.2 (Mutual information) The *mutual information* of two symbolic series X_S and Y_S , denoted as $I(X_S; Y_S)$, is defined as

$$I(X_S; Y_S) = \sum_{x \in \Sigma_X} \sum_{y \in \Sigma_Y} p(x, y) \cdot \log \frac{p(x, y)}{p(x) \cdot p(y)} \quad (9)$$

The MI represents the reduction of uncertainty of one variable (e.g., X_S), given the knowledge of another variable (e.g., Y_S). The larger $I(X_S; Y_S)$, the more information is shared between X_S and Y_S , and thus, the less uncertainty about one variable given the other.

We demonstrate how to compute the MI between the symbolic series S and T in Table 1. We have: $p(\text{Son}) = \frac{17}{36}$, $p(\text{Soff}) = \frac{19}{36}$, $p(\text{Ton}) = \frac{18}{36}$, and $p(\text{Toff}) = \frac{18}{36}$. We also have the joint probabilities: $p(\text{Son, Ton}) = \frac{15}{36}$, $p(\text{Soff, Toff}) = \frac{16}{36}$, $p(\text{Son, Toff}) = \frac{2}{36}$, and $p(\text{Soff, Ton}) = \frac{3}{36}$. Applying Eq. 9, we have $I(S; T) = 0.29$.

Since $0 \leq I(X_S; Y_S) \leq \min(H(X_S), H(Y_S))$ [10], the MI value has no upper bound. To scale the MI into the range $[0 - 1]$, we use normalized mutual information as defined below.

Definition 5.3 (Normalized mutual information) The *normalized mutual information* (NMI) of two symbolic time series X_S and Y_S , denoted as $\tilde{I}(X_S; Y_S)$, is defined as

$$\tilde{I}(X_S; Y_S) = \frac{I(X_S; Y_S)}{H(X_S)} = 1 - \frac{H(X_S|Y_S)}{H(X_S)} \quad (10)$$

$\tilde{I}(X_S; Y_S)$ represents the reduction (in percentage) of the uncertainty of X_S due to knowing Y_S . Based on Eq. (10), a pair of variables (X_S, Y_S) holds a mutual dependency if $\tilde{I}(X_S; Y_S) > 0$. Eq. (10) also shows that NMI is not symmetric, i.e., $\tilde{I}(X_S; Y_S) \neq \tilde{I}(Y_S; X_S)$.

Using Table 1, we have $I(S; T) = 0.29$. However, we do not know what the 0.29 reduction means in practice. Applying Eq. (10), we can compute $\text{NMI}(\tilde{I}(S; T)) = 0.43$, which says that the uncertainty of S is reduced by 43% given T . Moreover, we also have $\tilde{I}(T; S) = 0.42$, showing that $\tilde{I}(S; T) \neq \tilde{I}(T; S)$.

Definition 5.4 (Correlated symbolic time series) Let μ ($0 < \mu \leq 1$) be the mutual information threshold. We say that the two symbolic series X_S and Y_S are *correlated* iff $\tilde{I}(X_S; Y_S) \geq \mu \vee \tilde{I}(Y_S; X_S) \geq \mu$, and *uncorrelated* otherwise.

5.2 Lower Bound of the Confidence

5.2.1 Derivation of the lower bound. Consider 2 symbolic series X_S and Y_S . Let X_1 be a temporal event in X_S , Y_1 be a temporal event in Y_S , and \mathcal{D}_{SYB} and \mathcal{D}_{SEQ} be the symbolic and the sequence databases created from X_S and Y_S , respectively. We first study the relationship between the support of (X_1, Y_1) in \mathcal{D}_{SYB} and \mathcal{D}_{SEQ} .

LEMMA 8. Let $\text{supp}(X_1, Y_1)_{\mathcal{D}_{\text{SYB}}}$ and $\text{supp}(X_1, Y_1)_{\mathcal{D}_{\text{SEQ}}}$ be the support of (X_1, Y_1) in \mathcal{D}_{SYB} and \mathcal{D}_{SEQ} , respectively. We have the following relation: $\text{supp}(X_1, Y_1)_{\mathcal{D}_{\text{SYB}}} \leq \text{supp}(X_1, Y_1)_{\mathcal{D}_{\text{SEQ}}}$.

From Lemma 8, if an event pair is frequent in \mathcal{D}_{SYB} , it is also frequent in \mathcal{D}_{SEQ} . We now investigate the connection between $\tilde{I}(X_S; Y_S)$ in \mathcal{D}_{SYB} , and the confidence of (X_1, Y_1) in \mathcal{D}_{SEQ} .

THEOREM 1. (Lower bound of the confidence) Let σ and μ be the minimum support and mutual information thresholds, respectively. Assume that (X_1, Y_1) is frequent in \mathcal{D}_{SEQ} , i.e., $\text{supp}(X_1, Y_1)_{\mathcal{D}_{\text{SEQ}}} \geq \sigma$. If the NMI $\tilde{I}(X_S; Y_S) \geq \mu$, then the confidence of (X_1, Y_1) in \mathcal{D}_{SEQ} has a lower bound:

$$\text{conf}(X_1, Y_1)_{\mathcal{D}_{\text{SEQ}}} \geq \sigma \cdot \lambda_1^{\frac{1-\mu}{\sigma}} \cdot \left(\frac{n_x - 1}{1 - \sigma} \right)^{\frac{\lambda_2}{\sigma}} \quad (11)$$

where: n_x is the number of symbols in Σ_X , λ_1 is the minimum support of $X_i \in X_S$, and λ_2 is the support of $(X_i, Y_j) \in (X_S, Y_S)$ such that $p(X_i|Y_j)$ is minimal, $\forall (i \neq 1 \ \& \ j \neq 1)$.

PROOF. (Sketch - Please refer to the full paper [14] for a detailed proof). From Eq. (10), we have:

$$\tilde{I}(X_S; Y_S) = 1 - \frac{H(X_S|Y_S)}{H(X_S)} \geq \mu \quad (12)$$

$$\begin{aligned} \Rightarrow \frac{H(X_S|Y_S)}{H(X_S)} &= \frac{p(X_1, Y_1) \cdot \log p(X_1|Y_1)}{\sum_i p(X_i) \cdot \log p(X_i)} \\ &+ \frac{\sum_{i \neq 1 \ \& \ j \neq 1} p(X_i, Y_j) \cdot \log \frac{p(X_i, Y_j)}{p(Y_j)}}{\sum_i p(X_i) \cdot \log p(X_i)} \leq 1 - \mu \quad (13) \end{aligned}$$

Let $\lambda_1 = p(X_k)$ such that $p(X_k) = \min\{p(X_i)\} \forall i$, and $\lambda_2 = p(X_m, Y_n)$ such that $p(X_m|Y_n) = \min\{p(X_i|Y_j)\}, \forall (i \neq 1 \ \& \ j \neq 1)$. Then, by applying the min-max inequality theorem for the sum of ratio [5] to the numerator of Eq. (13), we obtain:

$$\begin{aligned} \frac{H(X_S|Y_S)}{H(X_S)} &\geq \frac{p(X_1, Y_1) \cdot \log p(X_1|Y_1) + \lambda_2 \cdot \log \frac{1-p(X_1, Y_1)}{n_x - p(Y_1)}}{\log \lambda_1} \\ &\geq \frac{\sigma \cdot \log \frac{p(X_1, Y_1)}{p(Y_1)} + \lambda_2 \cdot \log \frac{1-\sigma}{n_x - 1}}{\log \lambda_1} \quad (14) \end{aligned}$$

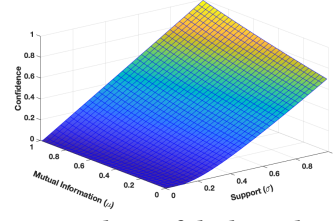


Figure 5: Shape of the lower bound

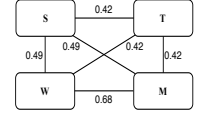


Figure 6: Corr. graph

Next, assume that $\text{supp}(Y_1)_{\mathcal{D}_{\text{SYB}}} \geq \text{supp}(X_1)_{\mathcal{D}_{\text{SYB}}}$. From Eqs. (13), (14), the confidence lower bound of (X_1, Y_1) in \mathcal{D}_{SYB} is derived as:

$$\text{conf}(X_1, Y_1)_{\mathcal{D}_{\text{SYB}}} = \frac{\text{supp}(X_1, Y_1)_{\mathcal{D}_{\text{SYB}}}}{\text{supp}(Y_1)_{\mathcal{D}_{\text{SYB}}}} \geq \lambda_1^{\frac{1-\mu}{\sigma}} \cdot \left(\frac{n_x - 1}{1 - \sigma} \right)^{\frac{\lambda_2}{\sigma}} \quad (15)$$

Since:

$$\text{conf}(X_1, Y_1)_{\mathcal{D}_{\text{SEQ}}} \geq \sigma \cdot \text{conf}(X_1, Y_1)_{\mathcal{D}_{\text{SYB}}} \quad (16)$$

It follows that:

$$\text{conf}(X_1, Y_1)_{\mathcal{D}_{\text{SEQ}}} \geq \sigma \cdot \lambda_1^{\frac{1-\mu}{\sigma}} \cdot \left(\frac{n_x - 1}{1 - \sigma} \right)^{\frac{\lambda_2}{\sigma}} \quad (17)$$

□

To compute the confidence lower bound in Eq. (11), several parameters need to be defined: n_x , λ_1 , λ_2 and μ . Here, we discuss how to determine the values of the first 3 parameters, and save the discussion of μ until Section 5.3. First, n_x is easily computed as the size of Σ_X . Second, λ_1 is the minimum support among all events $X_i \in X_S$, and λ_2 is the support of $(X_i, Y_j) \in (X_S, Y_S)$ such that $p(X_i|Y_j)$ is minimal, $\forall (i \neq 1 \ \& \ j \neq 1)$. The values of the three parameters can easily be determined given \mathcal{D}_{SYB} .

Interpretation of the confidence lower bound: Theorem 1 says that, given an MI threshold μ , if the two symbolic series X_S and Y_S are correlated, then the confidence of a frequent event pair in (X_S, Y_S) is at least the lower bound in Eq. (11). Combining Theorem 1 and Lemma 3, we can conclude that given (X_S, Y_S) , if its event pair has a confidence less than the lower bound, then any pattern P formed by that event pair also has a confidence less than that lower bound. This allows to approximate HTPGM (discussed in Section 5.3).

5.2.2 Shape of the confidence lower bound. To understand how the confidence changes w.r.t. the support σ and the MI μ , we analyze its shape, shown in Fig. 5 (σ and μ vary between 0 and 1). First, it can be seen that the confidence lower bound has a *direct relationship* with σ and μ (one increases if the other increases and vice versa). While the *direct relationship* between the confidence and σ can be explained using Eq. (5), it is interesting to observe the connection between μ and the confidence. As the MI represents the correlation between two symbolic series, the larger the value of μ , the more correlated the two series. Thus, when the confidence increases together with μ , it implies that patterns with high confidence are more likely to be found in highly correlated series, and vice versa.

Fig. 5 also shows that, when σ is low, e.g., $\sigma < 0.1$, we obtain a very low value of the confidence lower bound regardless of μ value. This implies that the confidence is less sensitive to μ when the support is low. The opposite is obtained when the support is high, e.g., $\sigma > 0.1$, where we see a visible increase of the confidence lower bound as μ increases. This indicates that the "insensitive" area of the lower bound (when $\sigma \leq 0.1$) is less accurate than the "sensitive" area ($\sigma > 0.1$) when performing the approximate mining, as we will discuss in Section 6.

5.3 Using the Bound to Approximate HTPGM

5.3.1 Correlation graph. Using Theorem 1, we propose to approximate HTPGM by performing the mining only on *the set of correlated symbolic series* $\mathcal{X}_C \subseteq \mathcal{X}$. We first define the correlation graph.

Definition 5.5 (Correlation graph) A *correlation graph* is an *undirected graph* $G_C = (V, E)$ where V is the set of vertices, and E is the set of edges. Each vertex $v \in V$ represents one symbolic series $X_S \in \mathcal{X}_C$. There is an edge e_{uv} between a vertex u containing X_S , and a vertex v containing Y_S iff $\tilde{I}(X_S; Y_S) \geq \mu \vee \tilde{I}(Y_S; X_S) \geq \mu$.

Fig. 6 shows an example of the correlation graph G_C built from \mathcal{D}_{SYB} in Table 1. Here, each node corresponds to one electrical appliance. There is an edge between two nodes if their NMI is at least μ . The number on each edge is the NMI between two nodes.

Constructing the correlation graph: Given a symbolic database \mathcal{D}_{SYB} , the correlation graph G_C can easily be constructed by computing the NMI for each symbolic series pair, and comparing their NMI against the threshold μ . A symbolic series pair is included in G_C if their NMI is at least μ , and vice versa.

Setting the value of μ : While NMI can easily be computed using Eq. (10), it is not trivial how to set the value for μ . Here, we propose a method to determine μ using the lower bound in Eq. (11).

Recall that HTPGM relies on two user-defined parameters, the support threshold σ and the confidence threshold δ , to look for frequent temporal patterns. Based on the confidence lower bound in Theorem 1, we can derive μ using σ and δ as the following.

COROLLARY 1.1. *The confidence of an event pair $(X_1, Y_1) \in (X_S, Y_S)$ in \mathcal{D}_{SEQ} is at least δ if $\tilde{I}(X_S; Y_S)$ is at least μ , where:*

$$\mu \geq 1 - \sigma \cdot \log_{\lambda_1} \left(\frac{\delta}{\sigma} \cdot \left(\frac{1 - \sigma}{n_x - 1} \right)^{\frac{\lambda_2}{\sigma}} \right) \quad (18)$$

Note that μ in Eq. (18) only ensures that the event pair (X_1, Y_1) has a minimum confidence of δ . Thus, given (X_S, Y_S) , μ has to be computed for each event pair in (X_S, Y_S) . The final chosen μ value to be compared against $\tilde{I}(X_S; Y_S)$ is the minimum μ value among all the event pairs in (X_S, Y_S) .

5.3.2 Approximate HTPGM using the correlation graph. Using the correlation graph G_C , the approximate HTPGM is described in Algorithm 2. First, \mathcal{D}_{SYB} is scanned once to compute the probability of each single event and pair of events (line 2). Next, NMI and μ are computed for each pair of symbolic series (X_S, Y_S) in \mathcal{D}_{SYB} (lines 4-5). Then, only pairs whose $\tilde{I}(X_S; Y_S)$ or $\tilde{I}(Y_S; X_S)$ is at least μ are inserted into \mathcal{X}_C , and an edge between X_S and Y_S is created (lines 6-8). Next, at L_1 of HPG, only the correlated symbolic series in \mathcal{X}_C are used to mine frequent single events (lines 9-10). At L_2 , G_C is used to filter 2-event combinations: for each event pair (E_i, E_j) , we check whether there is an edge between their corresponding symbolic series in G_C . If so, we proceed by verifying the support and confidence of (E_i, E_j) as in the exact HTPGM (lines 11-13). Otherwise, (E_i, E_j) is eliminated from the mining of L_2 . From level L_k ($k \geq 3$) onwards, the exact HTPGM is used (lines 14-15).

5.3.3 Complexity analysis. To compute NMI and μ , we only have to scan \mathcal{D}_{SYB} once to calculate the probability for each single event and pair of events. Thus, the cost of NMI and μ computations is $|\mathcal{D}_{\text{SYB}}|$. On the other hand, the complexity of the exact HTPGM at L_1 and L_2 are $O(m^2 i^2 |\mathcal{D}_{\text{SEQ}}|^2) + O(m \cdot |\mathcal{D}_{\text{SEQ}}|)$ (Section 4.5). Thus, the approximate HTPGM is significantly faster than HTPGM.

Algorithm 2: Approximate HTPGM using MI

Input: A set of time series \mathcal{X} , an MI threshold μ , support threshold σ , confidence threshold δ
Output: The set of frequent temporal patterns P

- 1: convert \mathcal{X} to \mathcal{D}_{SYB} and \mathcal{D}_{SEQ} ;
- 2: scan \mathcal{D}_{SYB} to compute the probability of each event and event pair;
- 3: **foreach** pair of symbolic time series $(X_S, Y_S) \in \mathcal{D}_{\text{SYB}}$ **do**
- 4: compute $\tilde{I}(X_S; Y_S)$ and $\tilde{I}(Y_S; X_S)$;
- 5: compute μ ;
- 6: **if** $\tilde{I}(X_S; Y_S) \geq \mu \vee \tilde{I}(Y_S; X_S) \geq \mu$ **then**
- 7: insert X_S and Y_S into \mathcal{X}_C ;
- 8: create an edge between X_S and Y_S in G_C ;
- 9: **foreach** $X_S \in \mathcal{X}_C$ **do**
- 10: mine frequent single events from X_S ;
- 11: **foreach** event pair (E_i, E_j) in L_1 **do**
- 12: **if** there is an edge between X_S and Y_S in G_C **then**
- 13: mine frequent patterns for (E_i, E_j) ;
- 14: **if** $k \geq 3$ **then**
- 15: perform HTPGM using L_1 and L_2 ;

6 EXPERIMENTAL EVALUATION

We evaluate HTPGM (both exact and approximate), using real-world datasets from three application domains: smart energy, smart city, and sign language. The evaluation is both qualitative (to assess the quality of extracted patterns) and quantitative (to evaluate the scalability and efficiency of HTPGM). Due to space limitations, we only present here the most important results, and discuss other findings in the full paper [14].

6.1 Experimental Setup

Datasets: We use 3 *smart energy* datasets, NIST [13], UKDALE [17], and DataPort [12], all of which measure the energy/power consumption of electrical appliances in residential households. For the *smart city*, we use weather and vehicle collision data obtained from NYC Open Data Portal [9]. The datasets contain information about weather conditions, and the collision incidents in New York City. For *sign language*, we use the American Sign Language (ASL) datasets [22] containing annotated video sequences of different ASL signs and gestures. Table 4 summarizes their characteristics.

Baseline methods: Our exact method is referred to as E-HTPGM, and the approximate one as A-HTPGM. We use three baselines (described in Section 2): TPMiner [8], IEMiner [25], and H-DFS [24]. Since E-HTPGM and the baselines provide the same exact solutions, we use the 3 baselines only for the quantitative evaluation, and compare qualitatively only between E-HTPGM and A-HTPGM.

Infrastructure: All methods, E-HTPGM, A-HTPGM and the baselines are implemented in Python. The experiments are run on a virtual machine with AMD EPYC Processor 32 cores (2GHz) CPU, 256 GB main memory, and 1 TB storage.

6.2 Qualitative Evaluation

Our goal is to make sense and learn insights from extracted patterns. Table 6 lists some interesting patterns found in the datasets. We note that the listed support and confidence are for the corresponding patterns. However, for time information, when relevant, we show only the most frequently occurring time intervals of the patterns, although the mining captures all time intervals.

Patterns P1 - P9 are extracted from the energy datasets, showing how the residents are interacting with electrical devices in their houses. For example, P1 shows that a resident turns on the light upstairs in the early morning, and goes to the bathroom. Then, within a minute later, the microwave in the kitchen is turned on. This implies that there might be more than one person living in the house, in which while one resident is in the bathroom, the other is downstairs preparing breakfast. In P4, we see the hall entry light is turned on at late afternoon, indicating that the residents might just arrive home from work. They proceed to move around the house and the family begins to prepare dinner around 18:00 by activating the light and the kitchen plugs, together with the microwave a few minutes later. Such patterns provide information about the living habits of the residents, from which enable actionable energy optimization, for example, pre-heating hot shower water when surplus wind energy is available during the night.

A majority of patterns extracted from the *smart city* datasets are linked to normal weather conditions. For example, the pattern (*Medium Temperature - Low Wind Speed - High Visibility - No Rain - No Thunder - No Tornado*) \rightarrow (*No Injury - No Death*) shows that collision situations are less severe in normal weather conditions. Although such patterns occur frequently in the data, e.g., 80% support, they do not reveal useful information. To look for more interesting patterns, we filtered those that link to extreme weather events, and found an association between extreme weather and high collision severity. Such patterns, e.g., P10 - P15, often occur with low support but high confidence, implying that although the associations are rare, they happen with strong confidence.

Patterns P16 - P19 are extracted from the ASL dataset, showing the temporal relations between different linguistic signs and gestures. Such patterns are useful, for example, to enable auto translation from video to text. For instance, in P16, a negation sign would contain a left head tilt-side and a lowered eye-brows gesture. In P17, a Wh-question will contain a lowered eye-brows followed by a blinking eye-aperture. Note that the ASL dataset does not distinguish between different Wh-questions.

6.3 Quantitative Evaluation

6.3.1 Baselines comparison on real world datasets. We compare E-HTPGM and A-HTPGM with the baselines in terms of the runtime and memory usage. Tables 7 and 8 show the results on the energy and the smart city datasets. The quantitative results of other datasets are reported in the full paper [14].

As shown in Table 7, A-HTPGM achieves the best performance (both runtime and memory usage) among all methods, and E-HTPGM has better performance than the baselines. On the tested datasets, the range and average speedups of A-HTPGM compared to other methods are: [1.7-21.3] and 3.88 (E-HTPGM), [3.4-29.3] and 10.6 (TPMiner), [4.3-74.2] and 17.1 (IEMiner), and [5.4-111.9] and 22.9 (H-DFS). The speedups of E-HTPGM compared to the baselines are: [1.3-8.2] and 3.2 on average (TPMiner), [2.5-11.9] and 4.8 on avg. (IEMiner), and [2.6-18.4] and 6.3 on avg. (H-DFS). Note that the time to compute MI and μ for the NIST and the smart city datasets in Table 7 are 28.01 and 20.82 seconds, respectively.

Moreover, A-HTPGM is most efficient, i.e., achieves highest speedup and memory saving, when the support threshold is low,

e.g., $\sigma=20\%$. This is because typical datasets often contain many patterns with very low support and confidence. Thus, using A-HTPGM to prune uncorrelated series early helps save computational time and resources. However, the speedup comes at the cost of a small loss in accuracy (discussed in Sections 6.3.2 and 6.3.4).

In average, on the tested datasets, E-HTPGM consumes ~ 2.5 times less memory than the baselines due to the applied pruning techniques, while A-HTPGM uses ~ 4 times less memory than E-HTPGM and the baselines by pruning uncorrelated series.

6.3.2 Scalability evaluation on synthetic datasets. As discussed in Section 4, the complexity of HTPGM is driven by 2 main factors: (1) the number of temporal sequences, and (2) the number of attributes, i.e., time series. The evaluation on real-world datasets has shown that E-HTPGM and A-HTPGM outperform the baselines significantly in both runtimes and memory usage. However, to further assess their scalability, we scale these two factors on synthetic datasets to perform the scalability evaluation. Specifically, starting from the real-world datasets, we generate 10 times more sequences, and create up to 1000 synthetic attributes. We evaluate the scalability using 2 configurations: varying the number of sequences (Figs. 7, 8), and varying the number of attributes (Figs. 9, 10).

Figs. 7 and 8 show the runtimes of A-HTPGM, E-HTPGM and the baselines when the number of sequences changes (y-axis is in log scale). The range and average speedups of A-HTPGM w.r.t. other methods are: [1.6-9.8] and 4.2 (E-HTPGM), [2.3-14.2] and 5.9 (TPMiner), [3.9-31.8] and 12.5 (IEMiner), and [5.5-37.4] and 20.1 (H-DFS). In particular, A-HTPGM obtains even higher speedup for more sequences. Similarly, the range and average speedups of E-HTPGM are: [0.5-2.4] and 1.4 (TPMiner), [0.9-3.1] and 1.9 (IEMiner), and [1.2-3.6] and 2.2 (H-DFS).

Figs. 9 and 10 compare the runtimes of A-HTPGM with other methods when changing the number of attributes (y-axis is in log scale). It is seen that, A-HTPGM achieves even higher speedup with more attributes. The range and average speedups of A-HTPGM are: [2.5-5.9] and 4.1 (E-HTPGM), [3.6-16.1] and 9.8 (TPMiner), [5.1-26.2] and 16.6 (IEMiner), and [5.9-37.6] and 22.8 (H-DFS), and of E-HTPGM are: [1.1-1.8] and 1.4 (TPMiner), [1.3-2.9] and 1.8 (IEMiner), and [1.9-10.8] and 5.8 (H-DFS).

In Figs. 9 and 10, to illustrate the computation time for MI and μ , we add an additional bar chart for A-HTPGM. Each bar represents the runtime of A-HTPGM with two separate components: the time to compute MI and μ (top red), and the mining time (bottom blue). However, note that for each dataset, we only need to compute MI and μ once (the computed values are used across the mining process with different support and confidence thresholds). Thus, the times to compute MI and μ , for example, in Figs. 9a, 9b, and 9c, are added only for comparison and are not all actually used.

Note that for the NIST dataset, when $\sigma=\delta=20\%$, and the number of attributes grows to 1000, the 2 baselines IEMiner and H-DFS run out of memory and fail to complete. The scalability test shows that A-HTPGM and E-HTPGM can scale well on big datasets, both vertically (many sequences) and horizontally (many attributes).

Furthermore, the number of attributes and events pruned by A-HTPGM in the scalability test are provided in Table 5. Here, we can see that high confidence threshold leads to more attributes (events) to be pruned. This is because confidence has a direct relationship

Table 4: Characteristics of the Datasets

	NIST	UKDALE	DataPort	Smart City	ASL
# sequences	1460	1520	1460	1216	1908
# variables	49	24	21	26	25
# distinct events	98	48	42	130	173
# instances/seq.	55	190	49	162	20

Table 5: Pruned Attributes and Events from A-HTPGM

# Attr.	NIST						Smart City					
	# Pruned Attributes			# Pruned Events			# Pruned Attributes			# Pruned Events		
	20-20	20-50	20-80	20-20	20-50	20-80	20-20	20-50	20-80	20-20	20-50	20-80
200	23	55	83	46	110	166	11	27	43	27	87	135
400	37	101	157	74	202	314	17	49	81	57	197	309
600	45	141	225	90	282	450	32	80	128	96	316	492
800	54	182	294	108	364	588	41	105	169	129	429	669
1000	83	243	383	166	486	766	51	131	211	163	543	847

Table 6: Summary of Interesting Patterns

Patterns	Supp. (%)	Conf. (%)
(P1) ([05:58, 08:24] First Floor Lights) \geq ([05:58, 06:59] Upstairs Bathroom Lights) \geq ([05:59, 06:06] Microwave)	20	30
(P2) ([06:00, 07:01] Upstairs Bathroom Lights) \geq ([06:40, 06:46] Upstairs Bathroom Plugs)	30	55
(P3) ([18:00, 18:30] Lights Dining Room) \rightarrow ([18:31, 20:16] Children Room Plugs) \emptyset ([19:00, 22:31] Lights Living Room)	20	20
(P4) ([15:59, 16:05] Hallway Lights) \rightarrow ([17:58, 18:29] Kitchen Lights \geq ([18:00, 18:18] Plug In Kitchen) \geq ([18:08, 18:15] Microwave)	20	25
(P5) ([06:02, 06:19] Kitchen Lights) \rightarrow ([06:05, 06:12] Microwave) \emptyset ([06:09, 06:11] Kettle)	20	35
(P6) ([18:10, 18:15] Kitchen App) \rightarrow ([18:15, 19:00] Lights Plugs) \geq ([18:20, 18:25] Microwave) \rightarrow ([18:25, 18:55] Cooktop)	25	50
(P7) ([16:45, 17:30] Washer) \rightarrow ([17:40, 18:55] Dryer) \rightarrow ([19:05, 20:10] Dining Room Lights) \geq ([19:10, 19:30] Cooktop)	10	30
(P8) ([06:10, 07:00] Kitchen Lights) \geq ([06:10, 06:15] Kettle) \rightarrow ([06:30, 06:40] Toaster) \rightarrow ([06:45, 06:48] Microwave)	25	40
(P9) ([18:00, 18:25] Kitchen Lights) \geq ([18:00, 18:05] Kettle) \rightarrow ([18:05, 18:10] Microwave) \rightarrow ([19:35, 20:50] Washer)	20	40
(P10) Heavy Rain \geq Unclear Visibility \geq Overcast Cloudiness \rightarrow High Motorist Injury	5	30
(P11) Extremely Unclear Visibility \geq High Snow \geq High Motorist Injury	3	45
(P12) Very Strong Wind \rightarrow High Motorist Injury	5	40
(P13) Frost Temperature \rightarrow Medium Cyclist Injury	5	20
(P14) Strong Wind \rightarrow High Pedestrian Killed	4	30
(P15) Strong Wind \rightarrow High Motorist Killed	4	10
(P16) [2.12 seconds] Negation \geq [0.61 seconds] Left Head Tilt-side \geq [0.27 seconds] Lowered Eye-brows	5	10
(P17) [1.53 seconds] Wh-question \geq [0.36 seconds] Lowered Eye-brows \rightarrow [0.05 seconds] Blinking Eye-aperture	10	15
(P18) [1.69 seconds] Wh-question \geq [0.35 seconds] Right Head Tilt-side \geq [0.27 seconds] Lowered Eye-brows	5	5
(P19) [1.92 seconds] Wh-question \geq [0.82 seconds] Squint Eye-aperture \rightarrow [0.13 seconds] Forward Body Lean	1	5

Table 7: Runtime Comparison (seconds)

Supp. (%)	Methods	Conf. (%)					
		NIST			Smart City		
		20	50	80	20	50	80
20	H-DFS	57651.52	7064.89	1620.07	2516.64	223.47	10.27
	IEMiner	50821.32	6162.83	1472.16	1419.51	130.80	8.59
	TPMiner	29671.91	5872.69	1172.19	418.25	118.89	6.66
	E-HTPGM	9417.84	1098.75	298.29	136.53	46.42	3.38
	A-HTPGM	3101.93	348.55	108.70	63.35	11.23	1.64
50	H-DFS	14654.45	3649.99	906.62	453.47	88.32	9.82
	IEMiner	10526.32	3257.69	810.83	300.80	73.81	7.81
	TPMiner	7261.88	2671.17	709.17	118.89	37.54	6.14
	E-HTPGM	883.01	577.37	183.58	86.42	16.75	3.12
	A-HTPGM	335.36	249.96	95.78	4.05	3.09	1.79
80	H-DFS	2199.27	1197.57	799.37	13.27	8.39	4.41
	IEMiner	1920.59	1052.98	701.52	9.59	5.47	4.37
	TPMiner	1084.92	982.62	501.78	6.66	3.44	3.37
	E-HTPGM	286.49	237.67	160.65	3.38	1.96	1.67
	A-HTPGM	106.92	83.13	62.66	0.95	0.92	0.48

Table 8: Memory Usage Comparison (MB)

Supp. (%)	Methods	Conf. (%)					
		NIST			Smart City		
		20	50	80	20	50	80
20	H-DFS	34591.22	6581.79	3369.17	1293.28	470.49	107.89
	IEMiner	30816.42	6051.93	3002.83	1197.74	460.52	65.92
	TPMiner	17829.26	5892.10	2986.10	1002.82	254.26	61.23
	E-HTPGM	7739.28	3110.82	1093.01	807.41	167.85	46.13
	A-HTPGM	4009.80	1903.20	640.45	227.89	101.82	39.79
50	H-DFS	22637.10	4628.14	2316.16	1040.56	412.14	92.81
	IEMiner	18622.62	4012.98	2162.72	870.64	353.18	60.87
	TPMiner	9310.63	3361.72	2052.52	660.66	150.68	58.98
	E-HTPGM	2269.84	2008.93	1665.47	144.13	134.07	46.04
	A-HTPGM	1036.48	936.07	523.00	121.01	99.95	36.19
80	H-DFS	2069.62	1987.27	1356.78	249.78	139.59	63.65
	IEMiner	2019.63	1869.20	1285.62	149.45	119.83	59.59
	TPMiner	1503.93	1307.47	1052.83	119.59	69.91	58.63
	E-HTPGM	921.54	860.97	663.89	64.30	44.22	43.16
	A-HTPGM	468.20	378.14	318.19	40.08	37.09	30.39

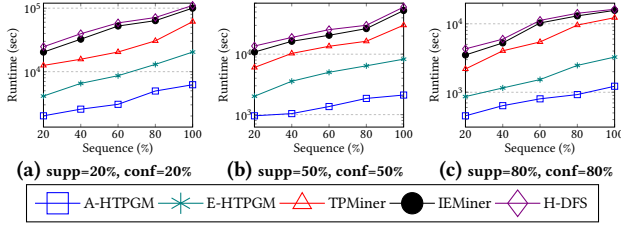
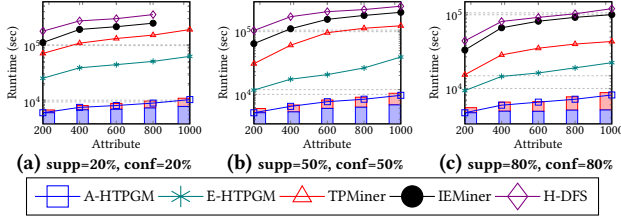
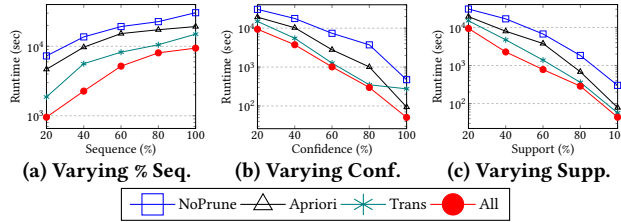
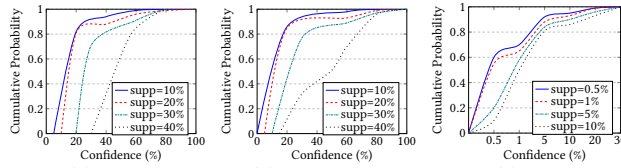
Table 9: The Accuracy and the Number of Extracted Patterns from A-HTPGM

Supp. (%)	Conf. (%)															
	NIST								Smart City							
	Accuracy (%)				# Patterns				Accuracy (%)				# Patterns			
	10	20	50	80	10	20	50	80	10	20	50	80	10	20	50	80
10	72	79	95	100	3379003	1609573	389609	40167	71	90	100	100	1441723	1231025	110559	34965
20	79	80	96	100	1596213	1557010	382695	40157	78	95	100	100	1291723	1201723	110491	34956
50	95	96	100	100	597685	547775	369102	40104	95	100	100	100	595462	520467	110409	34953
80	100	100	100	100	39821	39679	39526	39526	97	100	100	100	37366	37164	35074	34948

with MI, therefore, high confidence threshold results in higher μ , and thus, more pruned attributes.

6.3.3 *Evaluation of the pruning techniques in E-HTPGM.* We compare different versions of E-HTPGM to understand how effective

the pruning techniques are: (1) NoPrune: E-HTPGM with no pruning, (2) Apriori: E-HTPGM with Apriori-based pruning (Lemmas 2, 3), (3) Trans: E-HTPGM with transitivity-based pruning (Lemmas 4, 5, 6, 7), and (4) All: E-HTPGM applied both pruning techniques.

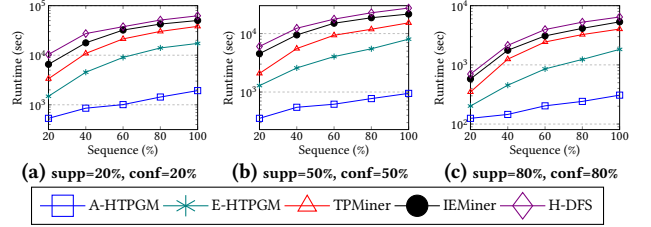
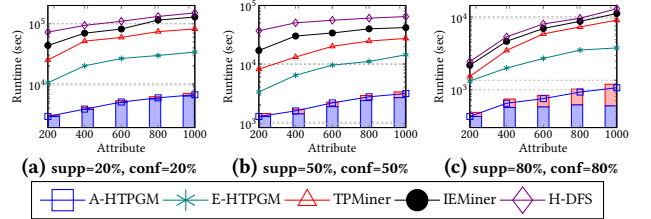
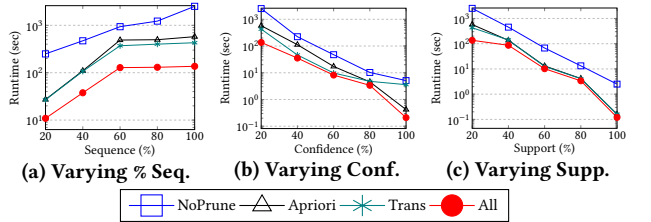

Figure 7: Varying % of sequences on NIST

Figure 9: Varying # of attributes on NIST

Figure 11: Runtimes of E-HTPGM on NIST

Figure 13: Cumulative probability of pruned patterns

We use 3 different configurations that vary: the number of sequences, the confidence, and the support. Figs. 11, 12 show the results (the y-axis is in log scale). It can be seen that (All)-E-HTPGM achieves the best performance among all versions. Its speedup w.r.t. (NoPrune)-E-HTPGM ranges from 5 up to 60 depending on the configurations, showing that the proposed prunings are very effective in improving E-HTPGM performance. Furthermore, (Trans)-E-HTPGM delivers larger speedup than (Apriori)-E-HTPGM. The average speedup is from 8 to 20 for (Trans)-E-HTPGM, and from 3 to 12 for (Apriori)-E-HTPGM. However, applying both always yields better speedup than applying either of them.

6.3.4 Evaluation of A-HTPGM. We proceed to evaluate the accuracy of A-HTPGM and the quality of patterns pruned by A-HTPGM.

To evaluate the accuracy, we compare the patterns extracted by A-HTPGM and E-HTPGM. Table 9 shows the accuracies of A-HTPGM and the numbers of extracted patterns for different supports and confidences. It is seen that, A-HTPGM obtains high accuracy ($\geq 70\%$) when σ and δ are low, e.g., $\sigma = \delta = 10\%$, and very high accuracy ($\geq 90\%$) when σ and δ are high, e.g., $\sigma = \delta = 50\%$.

Next, we analyze the quality of patterns pruned by A-HTPGM which are extracted from the uncorrelated time series. Fig. 13 shows


Figure 8: Varying % of sequences on Smart City

Figure 10: Varying # of attributes on Smart City

Figure 12: Runtimes of E-HTPGM on Smart City

the cumulative distribution of the confidences of the pruned patterns. It is seen that most of these patterns have low confidences, and can thus safely be pruned. For NIST and Smart City datasets, 80% of patterns have confidences less than 20% when the support is 10% and 20%, and 70% of patterns have confidences less than 30% when the support is 30%. For the ASL dataset, 80% of patterns have confidences less than 5%.

Other experiments: We analyze the effects of the tolerance buffer ϵ , and the overlapping duration t_{ov} to the quality of extracted patterns. The analysis can be seen in the full paper [14].

7 CONCLUSION AND FUTURE WORK

This paper presents our comprehensive Frequent Temporal Pattern Mining from Time Series (FTPMfTS) solution that offers: (1) an end-to-end FTPMfTS process to mine frequent temporal patterns from time series, (2) an efficient and exact Hierarchical Temporal Pattern Graph Mining (E-HTPGM) algorithm that employs efficient data structures and multiple pruning techniques to achieve fast mining, and (3) an approximate A-HTPGM that uses mutual information to prune unpromising time series, allows HTPGM to scale on big datasets. Extensive experiments conducted on real world and synthetic datasets show that both A-HTPGM and E-HTPGM outperform the baselines, consume less memory, and scale well to big datasets. Compared to the baselines, the approximate A-HTPGM delivers an order of magnitude speedup on large synthetic datasets and up to 2 orders of magnitude speedup on real-world datasets. In future work, we plan to extend HTPGM to prune at the event level to further improve its performance.

REFERENCES

- [1] Akiz Uddin Ahmed, Chowdhury Farhan Ahmed, Md Samiullah, Nahim Adnan, and Carson Kai-Sang Leung. 2016. Mining interesting patterns from uncertain databases. *Information Sciences* 354 (2016).
- [2] James F Allen. 1983. Maintaining knowledge about temporal intervals. *Commun. ACM* 26 (1983).
- [3] Iyad Batal, Dmitriy Fradkin, James Harrison, Fabian Moerchen, and Milos Hauskrecht. 2012. Mining recent temporal patterns for event detection in multivariate time series data. In *SIGKDD*.
- [4] Iyad Batal, Hamed Valizadegan, Gregory F Cooper, and Milos Hauskrecht. 2013. A temporal pattern mining approach for classifying electronic health record data. *TIST* 4 (2013).
- [5] Edwin F Beckenbach, Richard Bellman, and Richard Ernest Bellman. 1961. *An introduction to inequalities*. Technical Report. Mathematical Association of America Washington, DC.
- [6] Julien Blanchard, Fabrice Guillet, Regis Gras, and Henri Briand. 2005. Using information-theoretic measures to assess association rule interestingness. In *ICDM'05*.
- [7] Elizabeth A Campbell, Ellen J Bass, and Aaron J Masino. 2020. Temporal condition pattern mining in large, sparse electronic health record data: A case study in characterizing pediatric asthma. *JAMIA* 27 (2020).
- [8] Y. Chen, W. Peng, and S. Lee. 2015. Mining Temporal Patterns in Time Interval-Based Data. *TKDE* 27 (2015).
- [9] New York City. 2019. Nyc opendata. <https://opendata.cityofnewyork.us/>
- [10] Thomas M Cover and Joy A Thomas. 2012. *Elements of information theory*. John Wiley & Sons.
- [11] Xue Cunjin, Song Wanjiao, Qin Lijuan, Dong Qing, and Wen Xiaoyang. 2015. A mutual-information-based mining method for marine abnormal association rules. *Computers & Geosciences* 76 (2015).
- [12] Pecan Street Data. 2016. Pecan Street Dataport. <https://www.pecanstreet.org/dataport/>
- [13] William Healy, Farhad Omar, Lisa Ng, Tania Ullah, William Payne, Brian Dougherty, and A Hunter Fanney. 2018. Net zero energy residential test facility instrumented data. <https://pages.nist.gov/netzero/index.html>
- [14] Van Long Ho, Nguyen Ho, and Torben Bach Pedersen. 2020. Efficient Temporal Pattern Mining in Big Time Series Using Mutual Information. *arXiv preprint arXiv:2010.03653* (2020). <https://arxiv.org/abs/2010.03653>
- [15] Po-shan Kam and Ada Wai-Chee Fu. 2000. Discovering temporal patterns for interval-based events. In *DaWaK*.
- [16] Yiping Ke, James Cheng, and Wilfred Ng. 2008. Correlated pattern mining in quantitative databases. *TODS* 33 (2008).
- [17] Jack Kelly and William Knottenbelt. 2015. The UK-DALE dataset, domestic appliance-level electricity demand and whole-house demand from five UK homes. *Scientific Data* (2015).
- [18] Young-Koo Lee, Won-Young Kim, Y Dora Cai, and Jiawei Han. 2003. CoMine: Efficient Mining of Correlated Patterns. In *ICDM*.
- [19] Jessica Lin, Eamonn Keogh, Stefano Lonardi, and Bill Chiu. 2003. A symbolic representation of time series, with implications for streaming algorithms. In *Proceedings of the 8th ACM SIGMOD workshop on Research issues in data mining and knowledge discovery*. 2–11.
- [20] Vasileios Megalooikonomou, Qiang Wang, Guo Li, and Christos Faloutsos. 2005. A multiresolution symbolic representation of time series. In *21st International Conference on Data Engineering (ICDE'05)*. IEEE, 668–679.
- [21] Robert Moskovitch and Yuval Shahar. 2015. Fast time intervals mining using the transitivity of temporal relations. *KAIS* 42 (2015).
- [22] Carol Neidle, Augustine Opoku, Gregory Dimitriadis, and Dimitris Metaxas. 2018. NEW Shared & Interconnected ASL Resources: SignStream@ 3 Software; DAI 2 for Web Access to Linguistically Annotated Video Corpora; and a Sign Bank. In *8th Workshop on the Representation and Processing of Sign Languages: Involving the Language Community, Miyazaki, Language Resources and Evaluation Conference 2018*.
- [23] Edward R Omiecinski. 2003. Alternative interest measures for mining associations in databases. *IEEE Transactions on Knowledge and Data Engineering* 15, 1 (2003), 57–69.
- [24] Panagiotis Papapetrou, George Kollios, Stan Sclaroff, and Dimitrios Gunopulos. 2009. Mining frequent arrangements of temporal intervals. *KAIS* 21 (2009).
- [25] Dhaval Patel, Wynne Hsu, and Mong Li Lee. 2008. Mining relationships among interval-based events for classification. In *SIGMOD*.
- [26] Shin-Yi Wu and Yen-Liang Chen. 2007. Mining nonambiguous temporal patterns for interval-based events. *TKDE* 19 (2007).
- [27] YY Yao. 2003. Information-theoretic measures for knowledge discovery and data mining. In *Entropy measures, maximum entropy principle and emerging applications*. 115–136.

A DETAILED PROOFS OF COMPLEXITIES, LEMMAS AND THEOREMS

A.1 Mutual exclusive property of temporal relations

Property 1. (*Mutual exclusive*) Consider the set of temporal relations $\mathfrak{R} = \{\text{Follows}, \text{Contains}, \text{Overlaps}\}$. Let E_i and E_j be two temporal events, and e_i occurring during $[t_{s_i}, t_{e_i}]$, e_j occurring during $[t_{s_j}, t_{e_j}]$ be their corresponding event instances, and ϵ be the tolerance buffer. The relations in \mathfrak{R} are mutually exclusive on E_i and E_j .

PROOF. * **Case 1:** Assume the relation **Follows**($E_{i_{\rightarrow e_i}}, E_{j_{\rightarrow e_j}}$) holds between E_i and E_j . Thus, we have:

$$t_{e_i} \pm \epsilon \leq t_{s_j} \quad (19)$$

and:

$$t_{s_j} < t_{e_j} \Rightarrow t_{e_i} \pm \epsilon < t_{e_j} \quad (20)$$

Hence, **Contains**($E_{i_{\rightarrow e_i}}, E_{j_{\rightarrow e_j}}$) cannot exist between E_i and E_j , since **Contains**($E_{i_{\rightarrow e_i}}, E_{j_{\rightarrow e_j}}$) holds iff $(t_{s_i} \leq t_{s_j}) \wedge (t_{e_i} \pm \epsilon \geq t_{e_j})$ (contradict Eq. (20)).

Similarly, **Overlaps**($E_{i_{\rightarrow e_i}}, E_{j_{\rightarrow e_j}}$) cannot exist between E_i and E_j since **Overlaps**($E_{i_{\rightarrow e_i}}, E_{j_{\rightarrow e_j}}$) holds iff $(t_{s_i} < t_{s_j}) \wedge (t_{e_i} \pm \epsilon < t_{e_j}) \wedge (t_{e_i} - t_{s_j} \geq d_0 \pm \epsilon)$ (contradict Eq. (19)).

In conclusion, if **Follows**($E_{i_{\rightarrow e_i}}, E_{j_{\rightarrow e_j}}$) holds between E_i and E_j , then the two remaining relations cannot exist between E_i and E_j .

* **Case 2:** Assume the relation **Contains**($E_{i_{\rightarrow e_i}}, E_{j_{\rightarrow e_j}}$) holds between E_i and E_j . Thus, we have:

$$t_{s_i} \leq t_{s_j} \quad (21)$$

$$t_{e_i} \pm \epsilon \geq t_{e_j} \quad (22)$$

Hence, **Follows**($E_{i_{\rightarrow e_i}}, E_{j_{\rightarrow e_j}}$) cannot exist between E_i and E_j since **Follows**($E_{i_{\rightarrow e_i}}, E_{j_{\rightarrow e_j}}$) holds iff $t_{e_i} \pm \epsilon < t_{e_j}$ (contradict Eq. (22)).

Similarly, **Overlaps**($E_{i_{\rightarrow e_i}}, E_{j_{\rightarrow e_j}}$) cannot exist between E_i and E_j , since **Overlaps**($E_{i_{\rightarrow e_i}}, E_{j_{\rightarrow e_j}}$) holds iff $(t_{s_i} < t_{s_j}) \wedge (t_{e_i} \pm \epsilon < t_{e_j}) \wedge (t_{e_i} - t_{s_j} \geq d_0 \pm \epsilon)$ (contradict Eq. (22)).

In conclusion, if **Contains**($E_{i_{\rightarrow e_i}}, E_{j_{\rightarrow e_j}}$) holds between E_i and E_j , then the two remaining relations cannot exist between E_i and E_j .

* **Case 3:** Assume the relation **Overlaps**($E_{i_{\rightarrow e_i}}, E_{j_{\rightarrow e_j}}$) holds between E_i and E_j . Thus, we have:

$$t_{s_i} < t_{s_j} \quad (23)$$

$$t_{e_i} \pm \epsilon < t_{e_j} \quad (24)$$

$$t_{e_i} - t_{s_j} \geq d_0 \pm \epsilon \Rightarrow t_{s_j} \leq t_{e_i} - d_0 \pm \epsilon \quad (25)$$

Hence, **Follows**($E_{i_{\rightarrow e_i}}, E_{j_{\rightarrow e_j}}$) cannot exist between E_i and E_j , since **Follows**($E_{i_{\rightarrow e_i}}, E_{j_{\rightarrow e_j}}$) holds iff $t_{e_i} \pm \epsilon < t_{s_j}$ (contradict Eq. (25)).

Similarly, **Contains**($E_{i_{\rightarrow e_i}}, E_{j_{\rightarrow e_j}}$) cannot exist between E_i and E_j , since **Contains**($E_{i_{\rightarrow e_i}}, E_{j_{\rightarrow e_j}}$) holds iff $t_{e_i} \pm \epsilon \geq t_{e_j}$ (contradict Eq. (24)).

In conclusion, if **Overlaps**($E_{i_{\rightarrow e_i}}, E_{j_{\rightarrow e_j}}$) holds between E_i and E_j , then the two remaining relations cannot exist between E_i and E_j . \square

A.2 Mining frequent single event

Complexity: The complexity of finding frequent single events is $O(m \cdot |\mathcal{D}_{\text{SEQ}}|)$, where m is the number of distinct events.

PROOF. Computing the support for each event E_i takes $O(|\mathcal{D}_{\text{SEQ}}|)$ (to count the set bits of the *bitmap* b_{E_i} of length $|\mathcal{D}_{\text{SEQ}}|$). Thus, counting the support for m events takes $O(m \cdot |\mathcal{D}_{\text{SEQ}}|)$. \square

A.3 Lemma 1

Lemma 1. Let m be the number of distinct events in \mathcal{D}_{SEQ} , and h be the longest length of a temporal pattern. The total number of temporal patterns in HPG from L_1 to L_h is $O(m^h 3^{h^2})$.

PROOF. At L_1 , the number of nodes is: $N_1 = m \sim O(m)$. At L_2 , the number of permutations of m distinct events taken 2 at a time is: $P(m, 2)$. However, since the same event can form a pair of events with itself, e.g., (SON,SON), the total number of nodes at L_2 is: $N_2 = P(m, 2) + m \sim O(m^2)$. Each node in N_2 can form 3 different temporal relations, and thus, the total number of 2-event patterns in L_2 is: $N_2 \times 3^1 \sim O(m^2 3^1)$. Similarly, the number of 3-event nodes at L_3 is: $N_3 = P(m, 3) + P(m, 2) + m \sim O(m^3)$, and the number of 3-event patterns is: $N_3 \times 3^3 \sim O(m^3 3^3)$. At level L_h , the number of nodes is $O(m^h)$, while the number of h-event patterns is $O(m^h \times 3^{\frac{1}{2}h(h-1)}) \sim O(m^h 3^{h^2})$. Therefore, the total number of temporal patterns from L_1 to L_h in HPG is $O(m) + O(m^2 3^1) + O(m^3 3^3) + \dots + O(m^h 3^{h^2}) \sim O(m^h 3^{h^2})$. \square

A.4 Lemma 2

Lemma 2. Let P be a 2-event pattern formed by an event pair (E_i, E_j) . Then, $\text{supp}(P) \leq \text{supp}(E_i, E_j)$.

PROOF. Derived directly from Defs. 3.11, 3.12, 3.13 and 3.14. \square

A.5 Lemma 3

Lemma 3. Let (E_i, E_j) be a pair of events occurs in a 2-event pattern P . Then $\text{conf}(P) \leq \text{conf}(E_i, E_j)$.

PROOF. Can derived directly from Defs. 3.15 and 3.16. \square

A.6 Mining frequent 2-event pattern

Complexity: Let m be the number of frequent single events in L_1 , and i be the average number of event instances of each frequent event. The complexity of frequent 2-event pattern mining is $O(m^2 i^2 |\mathcal{D}_{\text{SEQ}}|^2)$.

PROOF. The Cartesian product of m events in L_1 generates m^2 event pairs. To compute the support of m^2 event pairs, we count the set bits of the *bitmap* that takes $O(m^2 |\mathcal{D}_{\text{SEQ}}|)$.

For each node in L_2 , we need to compute the support and confidence of their temporal relations, which takes $O(i^2 |\mathcal{D}_{\text{SEQ}}|^2)$. We have potentially m^2 nodes. And thus, it takes $O(m^2 i^2 |\mathcal{D}_{\text{SEQ}}|^2)$.

The overall complexity is: $O(m^2 |\mathcal{D}_{\text{SEQ}}| + m^2 i^2 |\mathcal{D}_{\text{SEQ}}|^2) \sim O(m^2 i^2 |\mathcal{D}_{\text{SEQ}}|^2)$. \square

A.7 Lemma 4

Lemma 4. Let $S = \langle e_1, \dots, e_{n-1} \rangle$ be a temporal sequence that supports an $(n-1)$ -event pattern $P = \langle (r_{12}, E_{1 \rightarrow e_1}, E_{2 \rightarrow e_2}), \dots, (r_{(n-2)(n-1)}, E_{n-2 \rightarrow e_{n-2}}, E_{n-1 \rightarrow e_{n-1}}) \rangle$. Let e_n be a new event instance added to S to create the temporal sequence $S' = \langle e_1, \dots, e_n \rangle$.

The set of temporal relations \mathfrak{R} is transitive on $S' : \forall e_i \in S', i < n, \exists r \in \mathfrak{R}$ s.t. $r(E_{i \rightarrow e_i}, E_{n \rightarrow e_n})$ holds.

PROOF. Since $S' = \langle e_1, \dots, e_n \rangle$ is a temporal sequence, the event instances in S' are chronologically ordered by their start times. Then, $\forall e_i \in S', i \neq n: t_{s_i} \leq t_{s_n}$. We have:

- If $t_{e_i} \pm \epsilon \leq t_{s_n}$, then $E_{i \rightarrow e_i} \rightarrow E_{n \rightarrow e_n}$.
- If $(t_{s_i} \leq t_{s_n}) \wedge (t_{e_i} \pm \epsilon \geq t_{e_n})$, then $E_{i \rightarrow e_i} \geq E_{n \rightarrow e_n}$.
- If $(t_{s_i} < t_{s_n}) \wedge (t_{e_i} \pm \epsilon < t_{e_n}) \wedge (t_{e_i} - t_{s_n} \geq d_o \pm \epsilon)$ where d_o is the minimal overlapping duration, then $E_{i \rightarrow e_i} \not\emptyset E_{n \rightarrow e_n}$. \square

A.8 Lemma 5

Lemma 5. Let $N_{k-1} = (E_1, \dots, E_{k-1})$ be a frequent $(k-1)$ -event combination, and E_k be a frequent single event. The combination $N_k = N_{k-1} \cup E_k$ can form frequent k -event temporal patterns if $\forall E_i \in N_{k-1}, \exists r \in \mathfrak{R}$ s.t. $r(E_i, E_k)$ is a frequent temporal relation.

PROOF. Let p_k be any k -event pattern formed by N_k . Then p_k is a list of $\frac{1}{2}k(k-1)$ triples (E_i, r_{ij}, E_j) where each represents a relation $r(E_i, E_j)$ between two events. In order for p_k to be frequent, each of the relations in p_k must be frequent (Defs. 3.11 and 3.15, and Lemma 4). However, since $\nexists E_i \in N_{k-1}$ such that $r(E_i, E_k)$ is frequent, p_k is not frequent. \square

A.9 Lemma 6

Lemma 6. Let P and P' be two temporal patterns. If $P' \subseteq P$, then $\text{conf}(P') \geq \text{conf}(P)$.

PROOF. Can be derived directly from Def. 3.16. \square

A.10 Lemma 7

Lemma 7. Let P and P' be two temporal patterns. If $P' \subseteq P$ and $\frac{\text{supp}(P')}{\max_{1 \leq k \leq |P|} \{\text{supp}(E_k)\}} \leq \delta$, then $\text{conf}(P) \leq \delta$.

PROOF. We have:

$$\begin{aligned} \text{conf}(P) &= \frac{\text{supp}(P)}{\max_{1 \leq k \leq |P|} \{\text{supp}(E_k)\}} \\ &\leq \frac{\text{supp}(P')}{\max_{1 \leq k \leq |P|} \{\text{supp}(E_k)\}} \leq \delta \end{aligned}$$

\square

A.11 Mining frequent k -event pattern

Complexity: Let r be the average number of frequent $(k-1)$ -event patterns in L_{k-1} . The complexity of frequent k -event pattern mining is $O(|\mathcal{I}\text{Freq}| \cdot |L_{k-1}| \cdot r \cdot k^2 \cdot |\mathcal{D}_{\text{SEQ}}|)$.

PROOF. For each frequent $(k-1)$ -event pattern of a node in L_k , we need to compute the support and confidence of $\frac{1}{2}(k-1)(k-2)$ triples, which takes $O(\frac{1}{2}(k-1)(k-2)|\mathcal{D}_{\text{SEQ}}|) \sim O(k^2|\mathcal{D}_{\text{SEQ}}|)$.

We have $|\mathcal{I}\text{Freq}| \times |L_{k-1}|$ nodes in L_k , each has r frequent $(k-1)$ -event patterns. Thus, the total complexity is: $O(|\mathcal{I}\text{Freq}| \cdot |L_{k-1}| \cdot r \cdot k^2 \cdot |\mathcal{D}_{\text{SEQ}}|)$. \square

A.12 Lemma 8

Lemma 8. Let $\text{supp}(X_1, Y_1)_{\mathcal{D}_{\text{SYB}}}$ and $\text{supp}(X_1, Y_1)_{\mathcal{D}_{\text{SEQ}}}$ be the supports of (X_1, Y_1) in \mathcal{D}_{SYB} and \mathcal{D}_{SEQ} , respectively. We have the following relation: $\text{supp}(X_1, Y_1)_{\mathcal{D}_{\text{SYB}}} \leq \text{supp}(X_1, Y_1)_{\mathcal{D}_{\text{SEQ}}}$.

PROOF. Recall that when converting \mathcal{D}_{SYB} to \mathcal{D}_{SEQ} , we divide the symbolic time series in \mathcal{D}_{SYB} into equal length temporal sequences. Let n be the length of each symbolic time series in \mathcal{D}_{SYB} , and m be the length of each temporal sequence. The number of temporal sequences obtained in \mathcal{D}_{SEQ} is: $\lceil \frac{n}{m} \rceil$.

The support of (X_1, Y_1) in \mathcal{D}_{SYB} is computed as:

$$\text{supp}(X_1, Y_1)_{\mathcal{D}_{\text{SYB}}} = \frac{\sum_{i=1}^{\lceil \frac{n}{m} \rceil} \sum_{j=1}^m s_{ij}}{n} \quad (26)$$

where

$$s_{ij} = \begin{cases} 1, & \text{if } (X_1, Y_1) \text{ occurs in row } j \text{ of the sequence } s_i \text{ in } \mathcal{D}_{\text{SYB}} \\ 0, & \text{otherwise} \end{cases}$$

Intuitively, Eq. 26 computes the relative support of (X_1, Y_1) in \mathcal{D}_{SYB} by counting the number of times (X_1, Y_1) occurs in \mathcal{D}_{SYB} , and then dividing to the size of \mathcal{D}_{SYB} .

On the other hand, the support of (X_1, Y_1) in \mathcal{D}_{SEQ} is computed by counting the number of sequences in \mathcal{D}_{SEQ} that (X_1, Y_1) occurs. Note that if (X_1, Y_1) occurs more than one in the same sequence, we will count only 1 for that sequence. Thus, we have:

$$\text{supp}(X_1, Y_1)_{\mathcal{D}_{\text{SEQ}}} = \frac{\sum_{i=1}^{\lceil \frac{n}{m} \rceil} g_i}{n/m} = \frac{m \cdot \sum_{i=1}^{\lceil \frac{n}{m} \rceil} g_i}{n} \quad (27)$$

where

$$g_i = \begin{cases} 1, & \text{if } (X_1, Y_1) \text{ occurs in the sequence } g_i \text{ in } \mathcal{D}_{\text{SEQ}} \\ 0, & \text{otherwise} \end{cases}$$

Compare Eqs. 26 and 27, we have:

$$\sum_{i=1}^{\lceil \frac{n}{m} \rceil} \sum_{j=1}^m s_{ij} \leq m \cdot \sum_{i=1}^{\lceil \frac{n}{m} \rceil} g_i \quad (28)$$

Hence:

$$\text{supp}(X_1, Y_1)_{\mathcal{D}_{\text{SYB}}} \leq \text{supp}(X_1, Y_1)_{\mathcal{D}_{\text{SEQ}}} \quad (29)$$

\square

A.13 Theorem 1

Theorem 1. (Lower bound of the confidence) Let σ and μ be the minimum support and mutual information thresholds, respectively. Assume that (X_1, Y_1) is frequent in \mathcal{D}_{SEQ} , i.e., $\text{supp}(X_1, Y_1)_{\mathcal{D}_{\text{SEQ}}} \geq \sigma$. If the NMI $\tilde{I}(\mathcal{X}_S; \mathcal{Y}_S) \geq \mu$, then the confidence of (X_1, Y_1) in \mathcal{D}_{SEQ} has a lower bound:

$$\text{conf}(X_1, Y_1)_{\mathcal{D}_{\text{SEQ}}} \geq \sigma \cdot \lambda_1^{\frac{1-\mu}{\sigma}} \cdot \left(\frac{n_x - 1}{1 - \sigma} \right)^{\frac{\lambda_2}{\sigma}} \quad (30)$$

where: n_x is the number of symbols in Σ_X , λ_1 is the minimum support of $X_i \in \mathcal{X}_S, \forall i$, and λ_2 is the support of $(X_i, Y_j) \in (\mathcal{X}_S, \mathcal{Y}_S)$ such that $\frac{p(X_i, Y_j)}{p(Y_j)}$ is minimal, $\forall (i \neq 1 \ \& \ j \neq 1)$.

PROOF. From Eq. (10), we have:

$$\tilde{I}(X_S; \mathcal{Y}_S) = 1 - \frac{H(X_S | \mathcal{Y}_S)}{H(X_S)} \geq \mu \quad (31)$$

Hence:

$$\frac{H(X_S | \mathcal{Y}_S)}{H(X_S)} \leq 1 - \mu \quad (32)$$

First, we derive a lower bound for $\frac{H(X_S | \mathcal{Y}_S)}{H(X_S)}$. We have:

$$\begin{aligned} \frac{H(X_S | \mathcal{Y}_S)}{H(X_S)} &= \frac{p(X_1, Y_1) \cdot \log p(X_1 | Y_1)}{\sum_i p(X_i) \cdot \log p(X_i)} \\ &+ \frac{\sum_{i \neq 1 \& j \neq 1} p(X_i, Y_j) \cdot \log \frac{p(X_i, Y_j)}{p(Y_j)}}{\sum_i p(X_i) \cdot \log p(X_i)} \end{aligned} \quad (33)$$

We first consider the numerator in Eq. (33). Suppose that:

$$\frac{p(X_m, Y_n)}{p(Y_n)} = \min\left\{\frac{p(X_i, Y_j)}{p(Y_j)}\right\}, \forall (i \neq 1 \& j \neq 1) \quad (34)$$

Then, applying the min-max inequality theorem [5], we have:

$$\frac{p(X_m, Y_n)}{p(Y_n)} \leq \frac{\sum_{i \neq 1 \& j \neq 1} p(X_i, Y_j)}{\sum_{i \neq 1 \& j \neq 1} p(Y_j)} = \frac{1 - p(X_1, Y_1)}{n_x - p(Y_1)} \quad (35)$$

$$\Rightarrow \log \frac{p(X_m, Y_n)}{p(Y_n)} \leq \log \frac{1 - p(X_1, Y_1)}{n_x - p(Y_1)} \quad (36)$$

$$\Rightarrow p(X_m, Y_n) \cdot \log \frac{p(X_m, Y_n)}{p(Y_n)} \leq p(X_m, Y_n) \cdot \log \frac{1 - p(X_1, Y_1)}{n_x - p(Y_1)} \quad (37)$$

Now, consider the second term of the numerator in Eq. (33). Since we have $\log \frac{p(X_i, Y_j)}{p(Y_j)} < 0$, hence:

$$\sum_{i \neq 1 \& j \neq 1} p(X_i, Y_j) \cdot \log \frac{p(X_i, Y_j)}{p(Y_j)} \leq p(X_m, Y_n) \cdot \log \frac{p(X_m, Y_n)}{p(Y_n)} \quad (38)$$

From Eqs (37), (38), it follows that:

$$\begin{aligned} \sum_{i \neq 1 \& j \neq 1} p(X_i, Y_j) \cdot \log \frac{p(X_i, Y_j)}{p(Y_j)} &\leq p(X_m, Y_n) \cdot \log \frac{1 - p(X_1, Y_1)}{n_x - p(Y_1)} \\ &= \lambda_2 \cdot \log \frac{1 - p(X_1, Y_1)}{n_x - p(Y_1)} \end{aligned} \quad (39)$$

where $\lambda_2 = p(X_m, Y_n)$.

Next, we consider the denominator in Eq. (33). Suppose that:

$$p(X_k) = \min\{p(X_i)\}, \forall i \quad (40)$$

Then we have:

$$\begin{aligned} p(X_i) &\geq p(X_k), \forall i \\ \Rightarrow \log p(X_i) &\geq \log p(X_k) \\ \Rightarrow p(X_i) \log p(X_i) &\geq p(X_i) \log p(X_k) \\ \Rightarrow \sum_i p(X_i) \log p(X_i) &\geq \sum_i p(X_i) \log p(X_k) \\ &= \log p(X_k) \sum_i p(X_i) \\ &= \log p(X_k) \\ &= \log \lambda_1 \end{aligned} \quad (41)$$

where $\lambda_1 = p(X_k)$.

Replace Eq. (39) and (41) into Eq. (33), we get:

$$\frac{H(X_S | \mathcal{Y}_S)}{H(X_S)} \geq \frac{p(X_1, Y_1) \cdot \log p(X_1 | Y_1) + \lambda_2 \cdot \log \frac{1 - p(X_1, Y_1)}{n_x - p(Y_1)}}{\log \lambda_1} \quad (42)$$

Next, we derive the confidence lower bound of (X_1, Y_1) in \mathcal{D}_{SYB} . Assuming that $\text{supp}(X_1, Y_1)_{\mathcal{D}_{\text{SEQ}}} \geq \text{supp}(X_1, Y_1)_{\mathcal{D}_{\text{SYB}}} \geq \sigma$. We consider two cases.

* **Case 1:** Assuming that $\text{supp}(Y_1)_{\mathcal{D}_{\text{SYB}}} \geq \text{supp}(X_1)_{\mathcal{D}_{\text{SYB}}}$. Thus, the confidence of (X_1, Y_1) in \mathcal{D}_{SYB} is computed as

$$\text{conf}(X_1, Y_1)_{\mathcal{D}_{\text{SYB}}} = \frac{\text{supp}(X_1, Y_1)_{\mathcal{D}_{\text{SYB}}}}{\text{supp}(Y_1)_{\mathcal{D}_{\text{SYB}}}} = \frac{p(X_1, Y_1)}{p(Y_1)} \quad (43)$$

Since we have: $\log \frac{p(X_1, Y_1)}{p(Y_1)} < 0$, and $\sigma \leq p(X_1, Y_1)$, we can deduce:

$$p(X_1, Y_1) \cdot \log \frac{p(X_1, Y_1)}{p(Y_1)} \leq \sigma \cdot \log \frac{p(X_1, Y_1)}{p(Y_1)} \quad (44)$$

We also have: $1 - p(X_1, Y_1) \leq 1 - \sigma$, and $n_x - 1 \leq n_x - p(Y_1)$, hence:

$$\begin{aligned} \frac{1 - p(X_1, Y_1)}{n_x - p(Y_1)} &\leq \frac{1 - \sigma}{n_x - 1} \\ \Rightarrow \lambda_2 \cdot \log \frac{1 - p(X_1, Y_1)}{n_x - p(Y_1)} &\leq \lambda_2 \cdot \log \frac{1 - \sigma}{n_x - 1} \end{aligned} \quad (45)$$

From Eqs. (44), (45), we have:

$$\begin{aligned} p(X_1, Y_1) \cdot \log \frac{p(X_1, Y_1)}{p(Y_1)} + \lambda_2 \cdot \log \frac{1 - p(X_1, Y_1)}{n_x - p(Y_1)} &\leq \\ \sigma \cdot \log \frac{p(X_1, Y_1)}{p(Y_1)} + \lambda_2 \cdot \log \frac{1 - \sigma}{n_x - 1} &\leq 0 \end{aligned} \quad (46)$$

Replace Eq. (46) into the numerator of Eq. (42), we get:

$$\frac{H(X_S | \mathcal{Y}_S)}{H(X_S)} \geq \frac{\sigma \cdot \log \frac{p(X_1, Y_1)}{p(Y_1)} + \lambda_2 \cdot \log \frac{1 - \sigma}{n_x - 1}}{\log \lambda_1} \quad (47)$$

From Eqs. (32) and (47), it follows that:

$$(1 - \mu) \geq \frac{\sigma \cdot \log \frac{p(X_1, Y_1)}{p(Y_1)} + \lambda_2 \cdot \log \frac{1 - \sigma}{n_x - 1}}{\log \lambda_1} \quad (48)$$

Hence:

$$\text{conf}(X_1, Y_1)_{\mathcal{D}_{\text{SYB}}} = \frac{p(X_1, Y_1)}{p(Y_1)} \geq \lambda_1^{\frac{1-\mu}{\sigma}} \cdot \left(\frac{n_x - 1}{1 - \sigma}\right)^{\frac{\lambda_2}{\sigma}} \quad (49)$$

* **Case 2:** Assuming that $\text{supp}(Y_1)_{\mathcal{D}_{\text{SYB}}} < \text{supp}(X_1)_{\mathcal{D}_{\text{SYB}}}$. Thus, the confidence of (X_1, Y_1) in \mathcal{D}_{SYB} is computed as

$$\text{conf}(X_1, Y_1)_{\mathcal{D}_{\text{SYB}}} = \frac{\text{supp}(X_1, Y_1)_{\mathcal{D}_{\text{SYB}}}}{\text{supp}(X_1)_{\mathcal{D}_{\text{SYB}}}} = \frac{p(X_1, Y_1)}{p(X_1)} \quad (50)$$

From Eq. (42), we have:

$$\frac{H(X_S | \mathcal{Y}_S)}{H(X_S)} \geq \frac{p(X_1, Y_1) \cdot \log \left(\frac{p(X_1, Y_1)}{p(X_1)} \cdot \frac{p(X_1)}{p(Y_1)}\right) + \lambda_2 \cdot \log \frac{1 - p(X_1, Y_1)}{n_x - p(Y_1)}}{\log \lambda_1} \quad (51)$$

$$\geq \frac{\sigma \cdot \log \left(\frac{p(X_1, Y_1)}{p(X_1)} \cdot \frac{1}{\sigma}\right) + \lambda_2 \cdot \log \frac{1 - \sigma}{n_x - 1}}{\log \lambda_1} \quad (52)$$

From Eqs. (32), (52), it follows that:

$$(1 - \mu) \geq \frac{\sigma \cdot \log \left(\frac{p(X_1, Y_1)}{p(X_1)} \cdot \frac{1}{\sigma} \right) + \lambda_2 \cdot \log \frac{1 - \sigma}{n_x - 1}}{\log \lambda_1} \quad (53)$$

Hence:

$$\text{conf}(X_1, Y_1)_{\mathcal{D}_{\text{SYB}}} = \frac{p(X_1, Y_1)}{p(X_1)} \geq \lambda_1^{\frac{1 - \mu}{\sigma}} \cdot \left(\frac{n_x - 1}{1 - \sigma} \right)^{\frac{\lambda_2}{\sigma}} \cdot \sigma \quad (54)$$

In Eq. (54), we have $\sigma < 1$. Thus, from Eqs. (49), (54), the confidence lower bound of (X_1, Y_1) in \mathcal{D}_{SYB} in both cases is:

$$\text{conf}(X_1, Y_1)_{\mathcal{D}_{\text{SYB}}} \geq \lambda_1^{\frac{1 - \mu}{\sigma}} \cdot \left(\frac{n_x - 1}{1 - \sigma} \right)^{\frac{\lambda_2}{\sigma}} \quad (55)$$

Next, we derive the confidence of (X_1, Y_1) in the temporal sequence database \mathcal{D}_{SEQ} . From Lemma 8, we have:

$$\text{supp}(X_1)_{\mathcal{D}_{\text{SYB}}} \leq \text{supp}(X_1)_{\mathcal{D}_{\text{SEQ}}} \quad (56)$$

$$\text{supp}(Y_1)_{\mathcal{D}_{\text{SYB}}} \leq \text{supp}(Y_1)_{\mathcal{D}_{\text{SEQ}}} \quad (57)$$

$$\text{supp}(X_1, Y_1)_{\mathcal{D}_{\text{SYB}}} \leq \text{supp}(X_1, Y_1)_{\mathcal{D}_{\text{SEQ}}} \quad (58)$$

Without loss of generality, we assume $\text{supp}(X_1)_{\mathcal{D}_{\text{SEQ}}} \geq \text{supp}(Y_1)_{\mathcal{D}_{\text{SEQ}}}$. Hence, the confidence of (X_1, Y_1) in \mathcal{D}_{SEQ} is computed as

$$\begin{aligned} \text{conf}(X_1, Y_1)_{\mathcal{D}_{\text{SEQ}}} &= \frac{\text{supp}(X_1, Y_1)_{\mathcal{D}_{\text{SEQ}}}}{\text{supp}(X_1)_{\mathcal{D}_{\text{SEQ}}}} \\ &\geq \frac{\text{supp}(X_1, Y_1)_{\mathcal{D}_{\text{SYB}}}}{\text{supp}(X_1)_{\mathcal{D}_{\text{SEQ}}}} \\ &= \frac{\text{supp}(X_1, Y_1)_{\mathcal{D}_{\text{SYB}}}}{\text{supp}(X_1)_{\mathcal{D}_{\text{SYB}}}} \cdot \frac{\text{supp}(X_1)_{\mathcal{D}_{\text{SYB}}}}{\text{supp}(X_1)_{\mathcal{D}_{\text{SEQ}}}} \\ &= \text{conf}(X_1, Y_1)_{\mathcal{D}_{\text{SYB}}} \cdot \frac{\text{supp}(X_1)_{\mathcal{D}_{\text{SYB}}}}{\text{supp}(X_1)_{\mathcal{D}_{\text{SEQ}}}} \quad (59) \end{aligned}$$

Since we have $\sigma \leq \text{supp}(X_1)_{\mathcal{D}_{\text{SYB}}}$ and $\text{supp}(X_1)_{\mathcal{D}_{\text{SEQ}}} \leq 1$, it follows that:

$$\frac{\text{supp}(X_1)_{\mathcal{D}_{\text{SYB}}}}{\text{supp}(X_1)_{\mathcal{D}_{\text{SEQ}}}} \geq \sigma \quad (60)$$

Finally, from Eqs. (55), (59) and (60), we can derive the confidence lower bound of (X_1, Y_1) in \mathcal{D}_{SEQ} :

$$\text{conf}(X_1, Y_1)_{\mathcal{D}_{\text{SEQ}}} \geq \sigma \cdot \lambda_1^{\frac{1 - \mu}{\sigma}} \cdot \left(\frac{n_x - 1}{1 - \sigma} \right)^{\frac{\lambda_2}{\sigma}} \quad (61)$$

□

B ADDITIONAL EXPERIMENTAL RESULTS

B.1 Baselines comparison

Tables 10 and 11 show the comparison results between A-HTPGM, E-HTPGM and the baselines on the UKDALE, DataPort, and ASL datasets. A-HTPGM achieves the best performance (both runtime and memory usage) among all methods, and E-HTPGM has better performance than the baselines. The range and average speedups of E-HTPGM compared to the baselines are: [2.1 – 7.7] and 3.4 (TPMiner), [3.1 – 13.2] and 6.2 (IEMiner), and [3.4 – 14.7] and

7.4 (H-DFS). Instead, the speedups of A-HTPGM compared to E-HTPGM and the baselines respectively are: [2.2 – 8.5] and 4.5 (E-HTPGM), [4.8 – 19.4] and 11.4 (TPMiner), [6.5 – 51.8] and 21.8 (IEMiner), and [7.8 – 60.9] and 25.9 (H-DFS). Note that the time to compute MI and μ for the UKDALE, DataPort, and ASL datasets in Table 10 are 17.82, 8.37, 11.27 seconds, respectively.

In average, on the tested datasets, E-HTPGM consumes ~ 2.1 times less memory than the baselines due to the applied pruning techniques, while A-HTPGM uses ~ 3.2 times less memory than E-HTPGM and the baselines by pruning uncorrelated series.

B.2 Evaluation of the pruning techniques in E-HTPGM

In this section, we report the evaluation results of E-HTPGM on UKDALE, DataPort and ASL datasets. We use 3 different configurations that vary: the number of sequences, the confidence, and the support. Figs. 14, 15, 16 show the results (the y-axis is in log scale). It can be seen that All-E-HTPGM achieves the best performance among all versions. Its speedup w.r.t. NoPrune-E-HTPGM ranges from 2.1 up to 7.6 depending on the configurations, showing that the proposed prunings are very effective in improving E-HTPGM performance. Furthermore, Trans-E-HTPGM brings larger speedup than Apriori-E-HTPGM. The speedup range is from 1.5 to 5.1 for Trans-E-HTPGM, and from 1.2 to 3.9 for Apriori-E-HTPGM. However, applying both always yields better speedup than applying either of them.

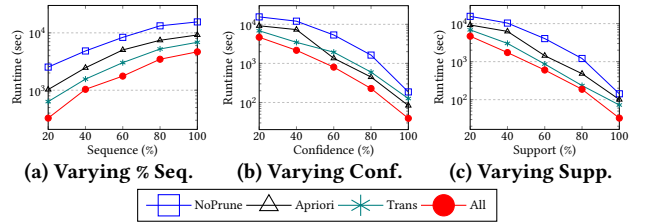


Figure 14: Runtimes of E-HTPGM on UKDALE

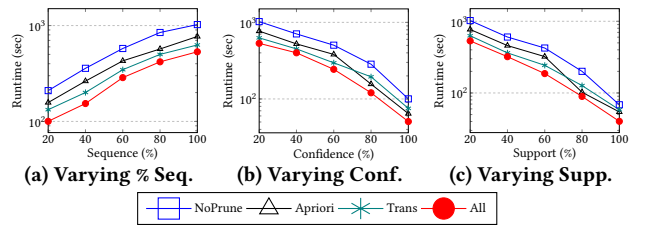


Figure 15: Runtimes of E-HTPGM on DataPort

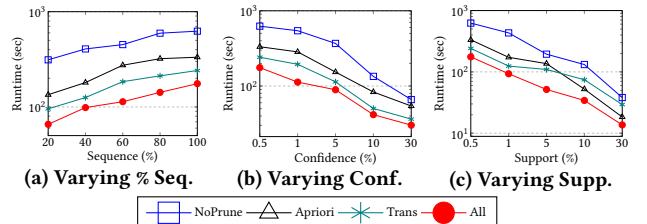


Figure 16: Runtimes of E-HTPGM on ASL

Table 10: Runtime Comparison (seconds)

Supp. (%)	Methods	Conf. (%)					
		UKDALE			DataPort		
		20	50	80	20	50	80
20	H-DFS	20130.09	3207.59	909.24	1802.76	1256.29	225.45
	IEMiner	15308.61	2841.64	816.51	1359.95	1006.34	208.62
	TPMiner	9045.28	2317.69	601.73	633.64	360.19	101.96
	E-HTPGM	4216.24	851.34	201.48	128.87	101.79	45.08
	A-HTPGM	1530.72	192.59	81.32	54.35	22.65	14.55
50	H-DFS	6208.26	1831.54	559.25	526.24	391.59	110.47
	IEMiner	5481.08	1570.18	426.13	460.37	321.78	93.64
	TPMiner	3251.94	1007.26	381.07	267.64	164.83	84.81
	E-HTPGM	420.18	237.29	110.54	80.14	57.39	30.25
	A-HTPGM	167.26	94.36	65.31	19.63	13.81	9.28
80	H-DFS	915.37	509.04	328.15	42.19	21.68	12.09
	IEMiner	852.81	454.26	294.38	35.09	16.95	10.36
	TPMiner	597.34	400.15	251.34	27.61	13.82	9.08
	E-HTPGM	138.92	103.58	94.21	5.69	4.07	2.94
	A-HTPGM	57.38	31.64	22.83	2.24	1.36	0.87

Supp. (%)	Methods	Conf. (%)		
		ASL		
		0.5	1	10
0.5	H-DFS	2028.32	1523.57	354.61
	IEMiner	1567.21	1307.83	301.53
	TPMiner	674.25	428.46	113.04
	E-HTPGM	175.74	112.74	41.65
	A-HTPGM	68.09	25.25	17.01
1	H-DFS	667.28	460.59	136.71
	IEMiner	547.63	384.03	116.27
	TPMiner	209.53	136.19	82.14
	E-HTPGM	93.13	63.18	35.69
	A-HTPGM	10.95	8.54	6.04
10	H-DFS	45.61	25.59	5.59
	IEMiner	40.27	21.91	5.07
	TPMiner	15.64	9.24	3.51
	E-HTPGM	4.22	2.03	1.33
	A-HTPGM	1.08	0.91	0.72

Table 11: Memory Usage Comparison (MB)

Supp. (%)	Methods	Conf. (%)					
		UKDALE			DataPort		
		20	50	80	20	50	80
20	H-DFS	13164.37	3258.19	1834.82	957.41	405.86	118.37
	IEMiner	11307.08	3014.82	1740.35	915.73	397.61	105.94
	TPMiner	7521.59	2641.58	1354.26	842.62	243.94	93.68
	E-HTPGM	4671.06	1903.64	928.38	532.47	184.62	84.72
	A-HTPGM	2038.47	873.46	435.27	416.52	91.03	58.41
50	H-DFS	8643.31	2257.36	1294.35	720.09	322.26	106.46
	IEMiner	7652.61	2010.53	1034.31	685.94	300.57	98.63
	TPMiner	3134.85	1623.25	921.08	469.33	219.63	91.54
	E-HTPGM	1051.36	936.91	543.16	230.61	154.36	76.61
	A-HTPGM	703.51	486.27	371.41	184.37	82.58	52.37
80	H-DFS	1943.05	1103.62	827.34	301.04	143.67	58.94
	IEMiner	1826.37	1004.31	807.92	297.62	120.83	52.63
	TPMiner	1406.52	867.38	759.37	172.93	112.54	43.82
	E-HTPGM	587.35	501.36	489.64	141.34	104.61	35.68
	A-HTPGM	340.58	247.92	203.18	108.31	68.72	34.26

Supp. (%)	Methods	Conf. (%)		
		ASL		
		0.5	1	10
0.5	H-DFS	1007.24	416.48	126.37
	IEMiner	946.81	409.21	120.54
	TPMiner	914.52	250.46	103.59
	E-HTPGM	723.51	150.08	89.52
	A-HTPGM	522.16	97.36	63.89
1	H-DFS	765.24	372.18	118.37
	IEMiner	713.48	351.22	110.73
	TPMiner	421.67	233.47	97.35
	E-HTPGM	246.81	129.41	54.03
	A-HTPGM	170.09	87.34	43.07
10	H-DFS	324.67	110.27	69.47
	IEMiner	318.32	107.33	60.45
	TPMiner	191.08	100.81	55.34
	E-HTPGM	145.21	59.34	50.14
	A-HTPGM	80.41	40.81	31.28

Table 12: The Accuracy and the Number of Extracted Patterns from A-HTPGM on UKDALE

Supp. (%)	Conf. (%)							
	UKDALE							
	Accuracy (%)				# Patterns			
	10	20	50	80	10	20	50	80
10	70	75	90	100	1647209	1058644	101327	20341
20	73	78	95	100	924612	842061	72649	15934
50	89	93	98	100	69367	62478	58326	13517
80	100	100	100	100	12584	11358	10659	10659

Table 13: The Accuracy and the Number of Extracted Patterns from A-HTPGM on DataPort

Supp. (%)	Conf. (%)							
	DataPort							
	Accuracy (%)				# Patterns			
	10	20	50	80	10	20	50	80
10	75	80	94	100	653225	226241	120654	9851
20	80	83	95	100	204587	184217	45462	8126
50	94	95	100	100	117562	100259	42096	7194
80	98	100	100	100	9051	8462	6428	5203

B.3 Evaluation of A-HTPGM

Table 12, 13, and 14 show the accuracies and the numbers of extracted patterns from A-HTPGM for different support and confidence thresholds. It can be seen that, A-HTPGM obtains high

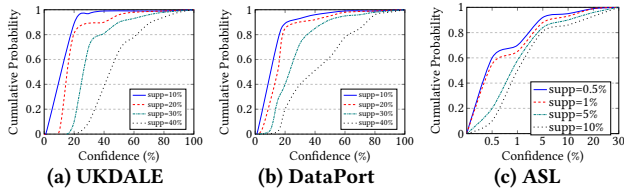
accuracy ($\geq 70\%$) when σ and δ are low, e.g. $\sigma = \delta = 10\%$, and very high accuracy ($\geq 90\%$) when σ and δ are high, e.g. $\sigma = \delta = 50\%$.

Next, we analyze the quality of patterns pruned by A-HTPGM. These patterns are extracted from the uncorrelated time series. Fig. 17 shows the cumulative distribution of the confidences for

Table 14: The Accuracy and the Number of Extracted Patterns from A-HTPGM on ASL

Supp. (%)	Conf. (%)							
	ASL				ASL			
	Accuracy (%)				# Patterns			
	0.5	1	5	10	0.5	1	5	10
0.5	82	85	95	98	86261	56747	3413	1960
1	87	87	95	100	24862	16561	3005	1902
5	91	97	100	100	5810	5612	1612	1484
10	94	98	100	100	1396	1106	1008	901

the pruned patterns. It is seen that most of these patterns have low confidences. For UKDALE and DataPort, 85% of patterns have confidences less than 20% when the support is 10% and 20%, and 75% of patterns have confidences less than 30% when the support is 30%. For ASL, 80% of patterns have confidences less than 5%. Such patterns are likely not interesting to explore, and thus, are pruned by A-HTPGM.

**Figure 17: Cumulative probability of pruned patterns**

B.4 Evaluation of the tolerance buffer ϵ

We evaluate the impact of the buffer ϵ on extracted patterns. Tables 15 and 16 report the number of extracted patterns for different ϵ values, and the corresponding percentages of pattern loss compared to $\epsilon = 0$. For NIST and DataPort datasets, the percentage of pattern loss is the lowest with $\epsilon = 1$ minute. For UKDALE, the percentage of pattern loss is the lowest with $\epsilon = 1$ and 2 minutes. And for Smart City, the percentage of pattern loss is very low, and the losses among different ϵ values are not very much different since there is low noise level in the dataset. For ASL, the percentage of pattern loss is the lowest when $\epsilon = 30$ frames.

Next, we analyze the quality of extracted patterns using different ϵ values. Specifically, for each specific ϵ value, we filter the patterns that are not in the result set of $\epsilon = 0$, and calculate the cumulative distribution of the confidences for them. Figs. 18 and 19 show the corresponding results on different datasets. For NIST and DataPort, 65% of patterns have confidences greater than 50% when ϵ is 1 minute, and 40% of patterns have confidences greater than 50% when ϵ is 2 and 3 minutes. For UKDALE, 60% of patterns have confidences greater than 50% when ϵ is 2 minutes, and 45% of patterns have confidences greater than 50% when ϵ is 1 and 3 minutes. For Smart City, 62% of patterns have confidences greater than 50% when ϵ is 10 minutes, and 49% of patterns have confidences greater than 50% when ϵ is 5 and 15 minutes. For ASL, 70% of patterns have confidences greater than 10% when epsilon is 30 frames, and 50% of patterns have confidences greater than 50% when epsilon is 45 and 60 frames.

Table 15: Number of Extracted Patterns and Percentages of Pattern Loss on NIST, UKDALE, and DataPort

ϵ value	NIST		UKDALE		DataPort	
	# Patterns	Patterns (%)	# Patterns	Patterns (%)	# Patterns	Patterns (%)
1 minute	1938081	0.42	1076811	0.31	220324	0.73
2 minutes	1864630	4.19	1076248	0.36	210348	5.22
3 minutes	1812857	6.85	1056532	2.18	202153	8.91

Table 16: Number of Extracted Patterns and Percentages of Pattern Loss on Smart City and ASL

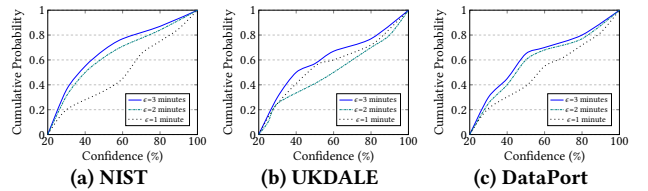
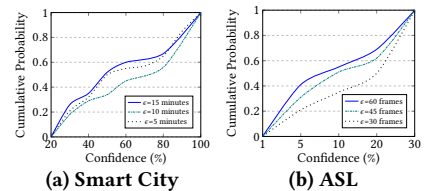
ϵ value	Smart City		ϵ value	ASL	
	# Patterns	Patterns (%)		# Patterns	Patterns (%)
5 minutes	1264207	0.06	30 frames	104627	0.54
10 minutes	1263902	0.08	45 frames	101683	3.34
15 minutes	1263787	0.09	60 frames	96475	8.29

Table 17: Number of Extracted Patterns with Different Overlapping Durations

Overlapping Duration	NIST	UKDALE	DataPort	Smart City	Overlapping Duration	ASL
0 hour	1946265	1080165	221948	1264971	0 frame	105196
1 hour	1947491	1084565	222052	1265193	150 frames	105302
2 hours	1947564	1085719	222052	1265232	300 frames	105302
3 hours	1947564	1085719	222052	1265232	450 frames	105302

B.5 Evaluation of the Splitting Strategy using Overlapping Sequences

We evaluate the impact of overlapping duration used in the sequences splitting strategy on extracted patterns. Table 17 reports the number of extracted patterns with different overlapping durations. For NIST, UKDALE, and Smart City, the number of extracted patterns increases when overlapping duration increases, and the number of extracted patterns becomes stable when the overlapping duration is equal to 2 hours or more. The same trend also applies for DataPort and ASL, where the number of extracted patterns becomes constant when overlapping duration is greater than 1 hour and 150 frames, respectively, for the two datasets.

**Figure 18: Cumulative probability of pattern loss****Figure 19: Cumulative probability of pattern loss**